iScience

CellPress
OPEN ACCESS

Article

Human RP105 monoclonal antibody enhances antigen-specific antibody production in unique culture conditions

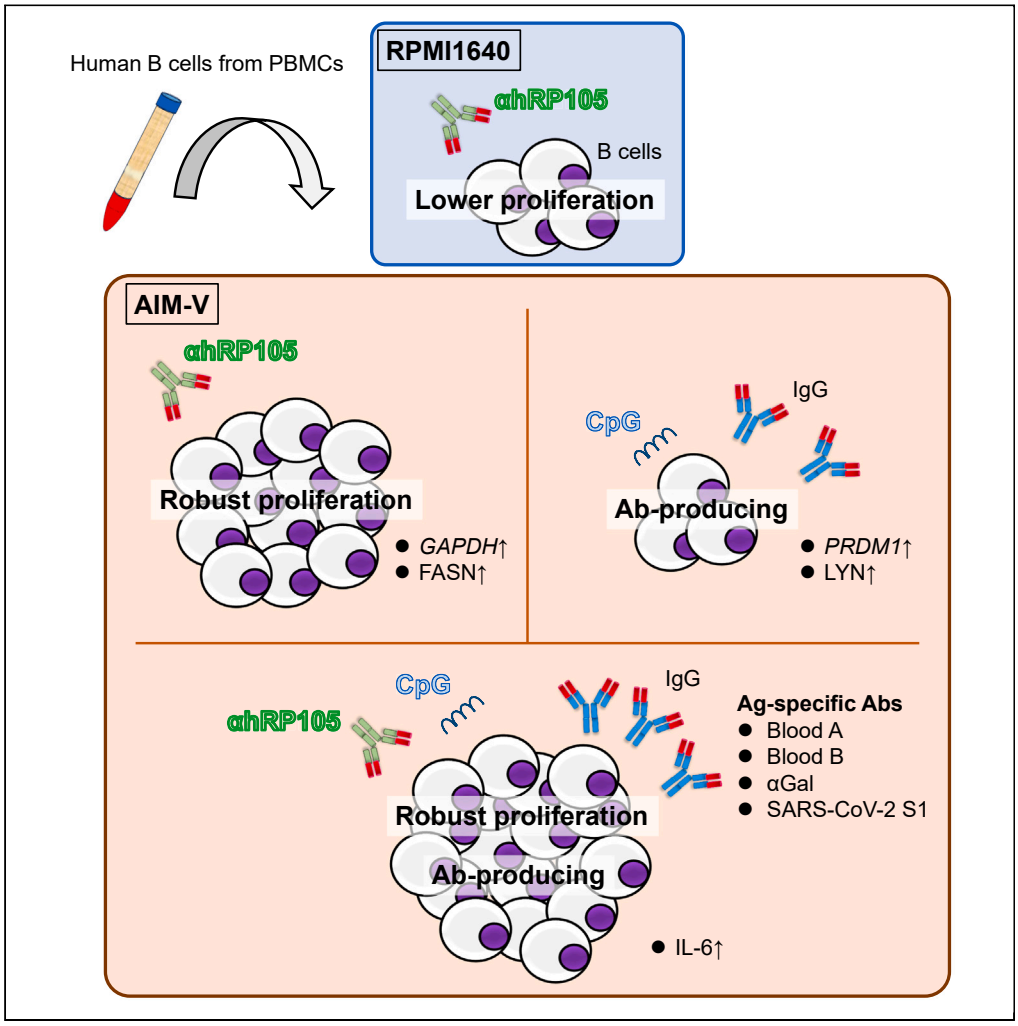

Tatsuya Yamazaki, Kenta Iwasaki, Susumu Tomono, ..., Manabu Okada, Takaaki Kobayashi, Sachiko Akashi-Takamura

kentaiwasaki@aichi-med-u.ac.jp (K.I.)
sachiko@aichi-med-u.ac.jp (S.A.-T.)

Highlights

Human B cells are strongly activated by αhRP105 alone in AIM-V medium

Comprehensive analysis reveals that αhRP105 triggers a different stimulus from CpGDNA

Human B cells produce antigen-specific antibodies by αhRP105 and CpGDNA addition

Yamazaki et al., iScience 27, 110649
September 20, 2024
https://doi.org/10.1016/j.isci.2024.110649

iScience

CellPress
OPEN ACCESS

Article

Human RP105 monoclonal antibody enhances antigen-specific antibody production in unique culture conditions

Tatsuya Yamazaki,[1,7] Kenta Iwasaki,[2,7,8,*] Susumu Tomono,[1] Masaki Imai,[3] Yuko Miwa,[2] Masato Shizuku,[4] Satoshi Ashimine,[4] Kohei Ishiyama,[4] Masanori Inui,[1] Daisuke Okuzaki,[5] Manabu Okada,[6] Takaaki Kobayashi,[4] and Sachiko Akashi-Takamura[1,*]

SUMMARY

Detecting antibodies, particularly those targeting donor human leukocyte antigens in organ transplantation and self-antigens in autoimmune diseases, is crucial for diagnosis and therapy. Radioprotective 105 (RP105), a Toll-like receptor family protein, is expressed in immune-competent cells, such as B cells. Studies in mice have shown that the anti-mouse RP105 antibody strongly activates B cells and triggers an adjuvant effect against viral infections. However, the anti-human RP105 antibody (αhRP105) weakly activates human B cells. This study established new culture conditions under, which human B cells are strongly activated by the αhRP105. When combined with CpGDNA, specific antibody production against blood group carbohydrates, αGal, and SARS-CoV-2 was successfully detected in human B cell cultures. Furthermore, comprehensive analysis using liquid chromatography-electrospray ionization tandem mass spectrometry, single-cell RNA sequencing, and quantitative real-time PCR revealed that αhRP105 triggered a different activation stimulus compared to CpGDNA. These findings could help identify antibody-producing B cells in cases of transplant rejection and autoimmune diseases.

INTRODUCTION

Radioprotective 105 (RP105, CD180), a type I transmembrane protein belonging to the Toll-like receptor (TLR) family, possesses a short cytoplasmic tail lacking the Toll-interleukin (IL)-1 receptor domain. This domain is essential for mediating TLR signaling, contributing to foreign pathogen recognition, and activation of the immune system activation across various species.[1–4] RP105 remains stably expressed on the cell surface by forming a complex with a soluble glycoprotein, myeloid differentiation 1 (MD-1), in humans and mice.[5,6] We recently found that human RP105 (hRP105) exhibits two forms depending on MD-1 and its two N-glycosylation sites (N96 and N156).[7] When mutant MD-1 (N96Q/N156Q) was present, the cell surface expression of hRP105 reduced, and MD-1 lacking glycosylation reduced the *de novo* cell surface expression of hRP105 on human embryonic kidney 293T cells.[7] Although RP105 is strongly expressed in B cells, macrophages, and dendritic cells, its ligand remains unidentified.[4,8] In a NZBWF1 mouse model, which shares pathogenic features with human systemic lupus erythematosus,[9,10] mouse RP105 (mRP105)-negative B cells infiltrated renal lesions and produced anti-double strand DNA antibodies. Further, hRP105-negative B cells have been shown to be associated with autoantibody production.[11,12] The number of hRP105-negative B cells increases in correlation with the disease activity, and decreases as the condition improves with treatment, making it a potential therapeutic marker.[13] However, reports of hRP105 molecules in human diseases remain scarce, and even in the previous cases, our knowledge of the function of hRP105 molecules remains limited.

Agonistic anti-mRP105 monoclonal antibodies (αmRP105, clone name: RP/14) crosslink with mRP105, inducing robust proliferation and antibody production in mouse B cells.[3] We have previously demonstrated the adjuvant effect of αmRP105 on antigen-specific antibody responses when vaccinating against infectious diseases in a mouse model.[14] Vaccination is crucial in the ongoing global spread of SARS-CoV-2.[15,16] However, in patients undergoing immunosuppressive therapies (e.g., organ transplantation)[17,18] and those with autoimmune diseases,[19] the rate of antibody acquisition after vaccination is significantly lower than in healthy individuals. These patients remain vulnerable to

[1]Department of Microbiology and Immunology, Aichi Medical University School of Medicine, Nagakute, Aichi, Japan
[2]Department of Kidney Diseases and Transplant Immunology, Aichi Medical University School of Medicine, Nagakute, Aichi, Japan
[3]Department of Medical Technology and Sciences, Kyoto Tachibana University, Kyoto, Kyoto, Japan
[4]Department of Renal Transplant Surgery, Aichi Medical University School of Medicine, Nagakute, Aichi, Japan
[5]Laboratory of Human Immunology (Single Cell Genomics), WPI-IFReC, Osaka University, Suita, Osaka, Japan
[6]Department of Transplant and Endocrine Surgery, Japanese Red Cross Aichi Medical Center Nagoya Daini Hospital, Nagoya, Aichi, Japan
[7]These authors contributed equally
[8]Lead contact
*Correspondence: kentaiwasaki@aichi-med-u.ac.jp (K.I.), sachiko@aichi-med-u.ac.jp (S.A.-T.)
https://doi.org/10.1016/j.isci.2024.110649

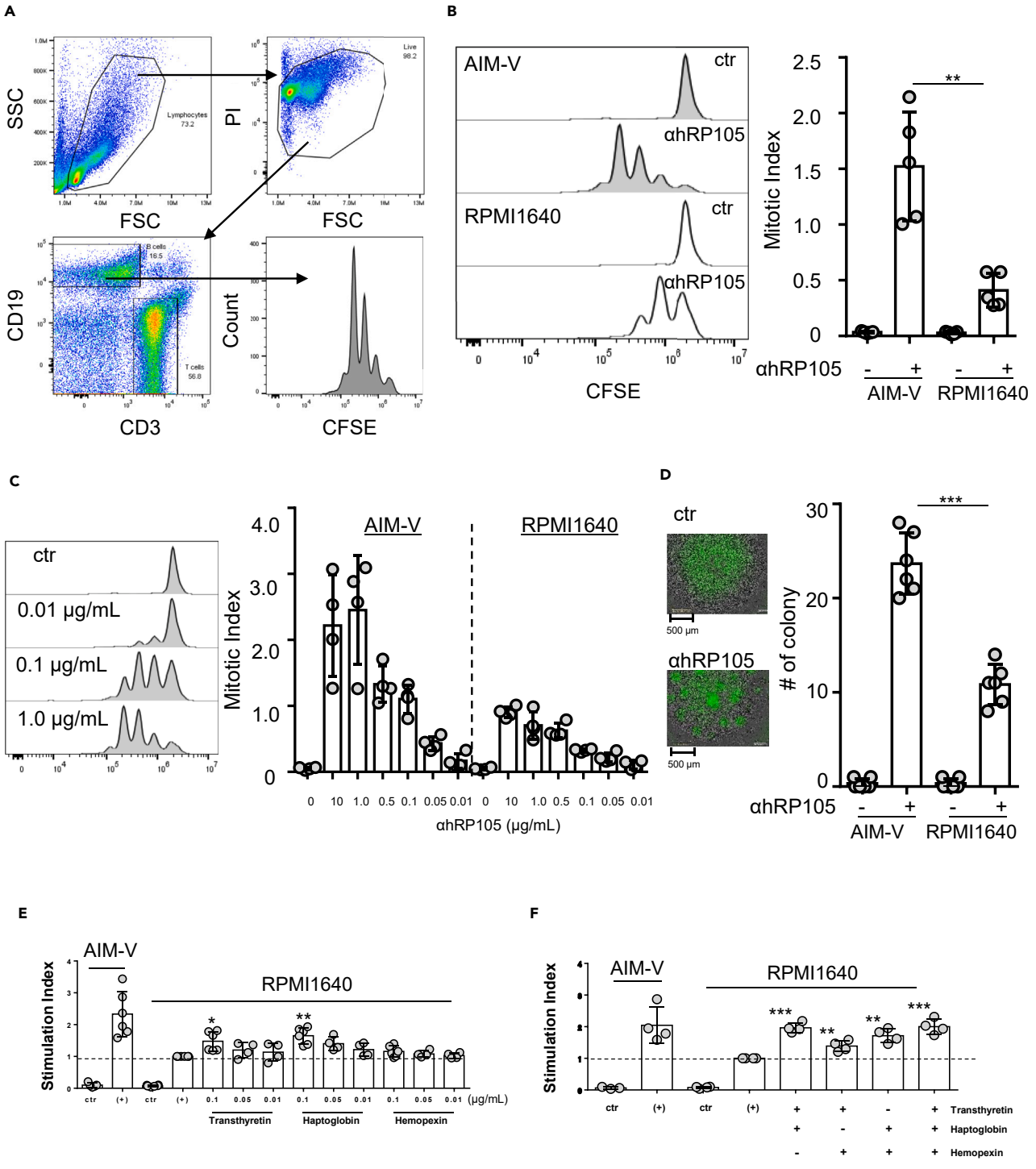

Figure 1. Enhanced human B cell proliferation stimulated with αhRP105 in AIM-V medium

(A) PBMCs from healthy volunteers were stained with CFSE and were stimulated with αhRP105 in either AIM-V or RPMI1640. Then, they were incubated for 3 days. A representative FCM gating strategy was shown how to evaluate the proliferation of $CD19^+$ B cells.

(B) Representative cell division of CFSE stained $CD19^+$ B-cells stimulated with 1.0 μg/mL of αhRP105 were shown on the left. The mitotic index calculated from proliferating $CD19^+$ B cells cultured in either AIM-V or RPMI1640 was shown on the right (n = 5).

(C) CFSE stained PBMCs were stimulated with various concentrations of αhRP105 in either AIM-V or RPMI1640. Representative cell division of CFSE-stained $CD19^+$ B cells stimulated with 0.01, 0.1, and 1.0 μg/mL of αhRP105 were shown on the left. The mitotic index calculated from proliferating $CD19^+$ B cells cultured in either AIM-V or RPMI1640 was shown on the right (n = 4).

Figure 1. *Continued*

(D) Purified CFSE stained CD19$^+$ B cells (Green color) in AIM-V were stimulated with αhRP105 for 3days in the IncuCyte ZOOM live cell imaging system. Representative cell clusters were shown on the left and their numbers were counted (right, $n = 6$).

(E and F) PBMCs from healthy volunteers were stained with CFSE and stimulated with αhRP105 in AIM-V or RPMI1640 in the presence of transthyretin (TTR), haptoglobin (HAP), hemopexin (HEM) alone (E) or in multiple doses respectively (F) for 3 days. The mitotic index and stimulation index calculated from proliferating CD19$^+$ B cells were shown (E: $n = 6$, F: $n = 4$). *$p < 0.05$, **$p < 0.01$, ***$p < 0.001$. Data are represented as mean ± SD.

infectious diseases underscoring the critical need for effective vaccines. Recent reports showed that RP105 represented one of the intriguing targets as a molecular adjuvant to enhance immune responses.[20] αmRP105 has been directly fused to the antigen hapten 4-hydroxy-3-nitrophenacetyl (NP) to act as a molecular adjuvant for boosting immune responses. NP-αmRP105 has been shown to induce a robust increase in polyclonal serum IgG titers and strong antigen-specific IgG and IgM immune response in mice.[21] Ag-specific IgG responses were also strongly observed in the ovalbumin (OVA)-αmRP105 group in comparison to OVA in alum controls and OVA-isotype controls.[22] These studies specifically target RP105 as a molecular adjuvant and suggest its potential as a vaccine adjuvant.

Despite the proposed utility of αmRP105, limited studies exist on the activation of human B cells by anti-hRP105 monoclonal antibodies (αhRP105, clone name: MHR73).[23] Notably, αhRP105 alone failed to induce strong proliferation and IgG production in CD27$^+$ memory human B cells.[24] When co-stimulated with the TLR9 ligand CpGDNA and retinoic acids, αhRP105 enhanced human B cell proliferation and IgG synthesis.[24,25] Specifically, it was suggested that the activation of B cells through RP105, particularly in conjunction with IL-21 and CpGDNA, led to IgM production even in common variable immunodeficiency (CVID) patients with reduced memory B cell.[26] Thus, αhRP105 can activate human B cells, which requires these supplements, such as retinoic acid or IL-21. Few studies have reported human B cell activation by αhRP105 alone. Overall, human B cell culture is delicate and challenging. Although the addition of numerous cytokines and the need for feeder cells has been reported, culture methods capable of stimulating the production of antigen-specific antibodies remain complex.[27–29]

In this study, we present a method to improve human B cell culture using αhRP105 alone and effectively expand human B cells through a culture medium useful for human immune cells.[30] Although using αhRP105 alone sufficiently induced cell proliferation, displaying greater potency than CpGDNA, combining these two stimulants more activated human B-cells. Under these conditions, the activation of human B cells by αhRP105 was confirmed through single-cell RNA sequencing (scRNA-seq) analysis and flow cytometry (FCM). The results showed an increase in the TLR family, cell-cycle, IL-6-related molecules, NF-κB family, and certain activation markers. Moreover, the induction of anti-ABO blood group, anti-αGal, and anti-SARS-CoV-2 S1 antibodies in the healthy volunteers vaccinated with either mRNA-1273 or BTN162b2 was also confirmed.

RESULTS

αhRP105 increased human CD19$^+$ B cell proliferation

Previous reports have shown that αhRP105 alone cannot effectively induce human B cell proliferation.[24,25] However, we observed more robust proliferation of CD19$^+$ human B cells in AIM-V medium compared to RPMI1640, using the carboxyfluorescein diacetate, succinimidyl ester (CFSE)-stained B cell proliferation method (Figure 1A). Additionally, a higher mitotic index was observed (1.52 ± 0.49 vs. 0.41 ± 0.15, $p < 0.01$, Figure 1B). Although the amount of αhRP105 is proportional to cell proliferation, the mitotic index at 10 μg/mL of αhRP105 stimulation in RPMI1640 was equivalent to that at 0.1 μg/mL in AIM-V (Figure 1C). Cell cluster formation induced by αhRP105 stimulation began 48 h poststimulation, with clear clusters forming after 72 h (see Figure S1). Significantly more cell clusters larger than 20 μm were observed in AIM-V cultures compared to RPMI1640 (23.7 ± 3.3 vs. 10.8 ± 2.2, $p < 0.001$) (Figure 1D). These results confirmed the efficient activation of CD19$^+$ B cell proliferation by αhRP105 in AIM-V medium. To determine which components of AIM-V contributed to the activation of human CD19$^+$ B cells, the protein components of the medium were examined. Among the proteins identified in the AIM-V medium through LC/ESI-MS/MS (data not shown), three proteins (transthyretin, haptoglobin, and hemopexin) were abundant and further investigated. In the experiment with CFSE-stained peripheral blood mononuclear cells (PBMCs) stimulated with αhRP105 in RPMI1640 supplemented with these proteins, transthyretin and haptoglobin enhanced CD19$^+$ B cell proliferation, respectively, whereas hemopexin exhibited only marginal effects (with no significant difference) (Figure 1E). CD19$^+$ B cells proliferated when transthyretin and haptoglobin were combined (Figure 1F), whereas the effect of hemopexin remained limited (Figure 1F). These findings highlight the efficacy of AIM-V medium in activating human CD19$^+$ B cells by αhRP105 and the potential significance of transthyretin and haptoglobin in this process.

Gene regulation in human B cells activated by αhRP105

To investigate gene regulation under optimal conditions for CD19$^+$ B cell activation with αhRP105, PBMCs from three healthy volunteers were cultured with αhRP105 for 36 h. Subsequently, CD19$^+$CD20$^+$ cells were collected using a cell sorter for scRNA-seq analysis (Figure 2A, left). Nine clusters were identified using Uniform Manifold Approximation and Projection (UMAP), separating nonactivated and activated B cells (see Figure S2). UMAP embedding and clustering enabled the identification of clusters comprising both nonactivated and activated CD19$^+$ B cells (Figure 2A, right). The single-cell bubble plot data showed an increase in the expression of costimulatory molecules (CD86 and CD40), TLR family members (TLR9 and TLR10), MD-1/2 (LY86/LY96), the IL-6 receptor (IL-6R), IL-6 signal transduction (IL6ST), cell cycle-related genes (cyclin D2 (CCND2), CDK4, PCNA, SMAD3, and FOXO1), and NF-κB family members (NF-κB1, NF-κB2, RelA, and RelB) in activated CD19$^+$ B cells (Figure 2B). Additionally, AKT, a cell survival signal, increased upon αhRP105 stimulation (see Figure S3). To validate the expression of CD19$^+$ B cell activation markers at the protein levels, CD80 and CD38 were measured during cell proliferation experiments. Although the

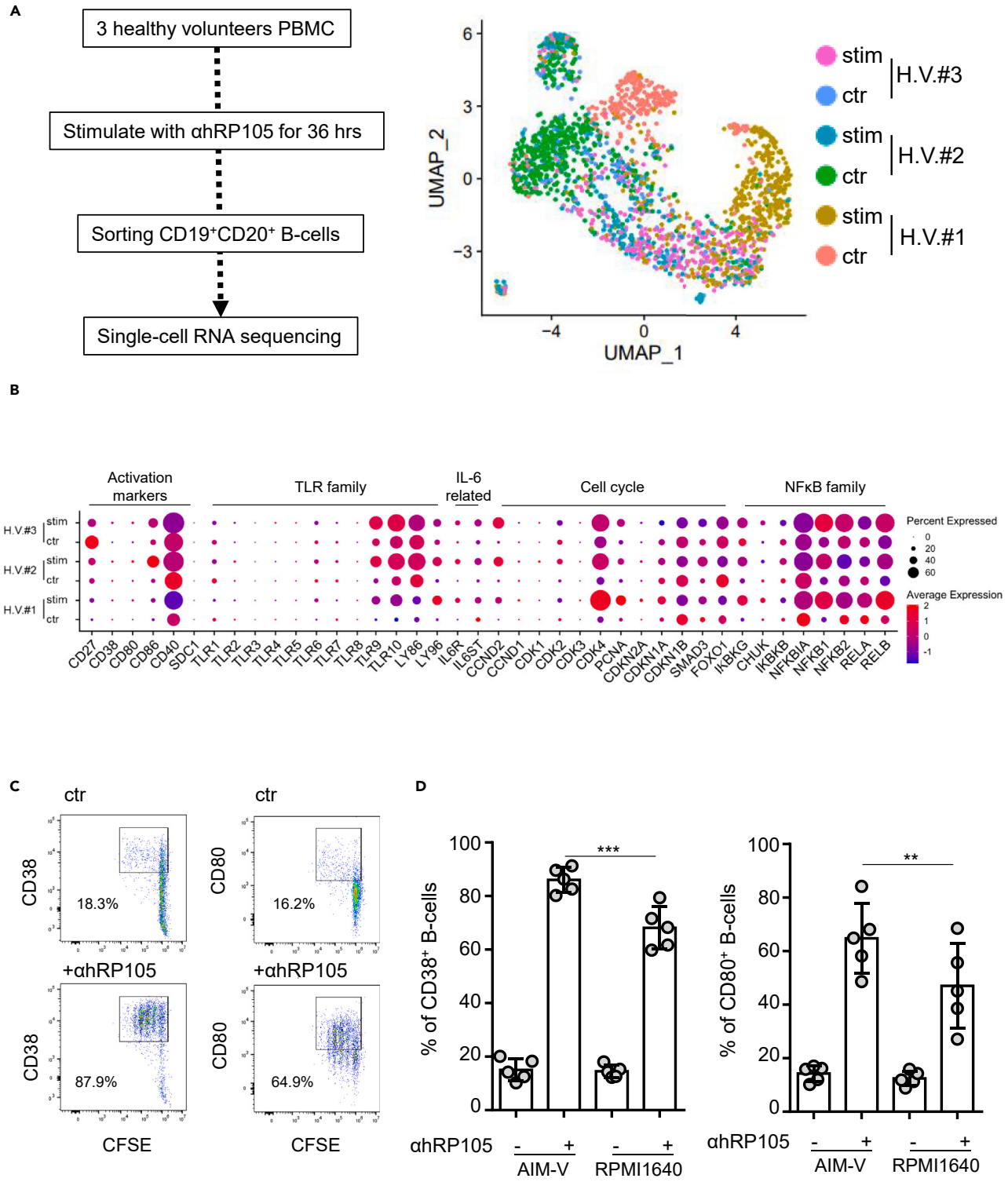

Figure 2. Enhanced human B cell activation by αhRP105

(A) The flowchart of this experiment was shown. PBMCs from three healthy volunteers (H.V.#1, H.V.#2, and H.V.#3) were stimulated or unstimulated with αhRP105 for 36 h (total 6 samples) in AIM-V medium. Each PBMCs were stained with hashtag antibodies, then were stained with anti-CD19 and anti-CD20 antibodies. B cells were sorted, pooled, and analyzed by scRNA-seq. A UMAP consisting of six samples from three healthy volunteers were shown.

(B) The expression of costimulatory molecules, TLR family, IL-6-related genes, cell cycle genes, and NF-κB family were shown as bubble plots.

Figure 2. *Continued*

(C) PBMCs from healthy volunteers were stained with CFSE and were stimulated with 1.0 μg/mL of αhRP105 in AIM-V for 3days. The expression of CD38 and CD80 activation markers was evaluated by FCM. A representative FCM was shown how to evaluate the expression of CD38 and C80 in proliferated $CD19^+$ B cells.
(D) Each activation marker positive rate from $CD19^+$ B cells was shown ($n = 5$). $^{**}p < 0.01$, $^{***}p < 0.001$. Data are represented as mean ± SD.

percentage expression of CD38 and CD80 genes was low after 36 h incubation (Figure 2B), representative FCM experiments of 3 days cultured cells demonstrated that the expression of these proteins increased by over 80% and 60%, respectively (Figure 2C). $CD19^+$ B cells cultured in AIM-V exhibited higher positivity for each protein expression than those in RPMI1640 (CD38: 86.0% ± 4.7% vs. 68.2% ± 7.9%, $p < 0.001$, CD80: 64.8% ± 13.2% vs. 47.0% ± 15.9%, $p < 0.01$, Figure 2D). These findings indicate that αhRP105-induced activation of $CD19^+$ B cells enhances the regulation of cell-cycle genes and increases the expression of $CD19^+$ B cell activation markers and costimulatory molecules.

Expression of hRP105 molecules on the human $CD19^+$ B cell surface

The expression of the hRP105 molecule in peripheral blood B cells was compared with that in T-cells and monocytes. The representative FCM gating strategy showed that hRP105 is expressed in $CD19^+$ B cells and $CD14^+$ monocytes, but not in $CD3^+$ T cells. Notably, the expression intensity of hRP105 was most pronounced in $CD19^+$ B cells (Figure 3A). Peripheral $CD19^+$ B cells were categorized into naive ($CD27^-IgD^+$), unswitched memory ($CD27^+IgD^+$), double-negative ($CD27^-IgD^-$), and switched memory ($CD27^+IgD^-$) cells. Surface markers such as CD10 (MME), CD38 and CD138 (SDC1) were used to segregate cells into transitional B cells, plasmablasts, and plasma cells.[31] Our scRNA-seq analysis showed only a small population expressing each gene expression in the nonactivated $CD19^+$ B cells (see Figure S4). Although these populations have been reported to have important functions, we decided to exclude them from the current evaluation. Most peripheral $CD19^+$ B cells were of the naive subtype (Figure 3B). hRP105 was expressed in almost all types of B cells (Figure 3C) and did not vary with age (Figure 3D). This trend was also observed in peripheral $CD19^+$ B cells from kidney transplant patients under immunosuppressive conditions (see Figure S5, transplant patient information is available in the Table S1). These findings indicate that hRP105 is consistently expressed on $CD19^+$ B cells regardless of the patient's age or immunosuppressive status.

$CD19^+$ B cell activation by CpGDNA and αhRP105 shows different gene expression patterns

A single-cell UMAP analysis of TLR family gene expression in $CD19^+$ B cells following αhRP105 stimulation revealed increased expression of TLR9 and TLR10 (Figure 2B). Given that αhRP105-mediated upregulation of TLR9 has been previously confirmed,[26] we compared the activation of purified $CD19^+$ B cells by αhRP105 and CpGDNA. The accuracy of $CD19^+$ B cell purification is shown in Figure S6A. Purified $CD19^+$ B cells proliferated with only 0.1 μg/mL of αhRP105, similar to the response seen with 1.0 μg/mL in PBMCs (see Figure S6B). CFSE-stained $CD19^+$ B cells were stimulated with αhRP105 and/or CpGDNA for 3 days Figure 4A presents representative discrete CFSE peaks denoting successive generations of live cells. Stimulation with αhRP105 yielded significantly higher cell proliferation compared to CpGDNA (mitotic index: 1.95 ± 0.56 vs. 0.37 ± 0.09, $p < 0.001$) (Figure 4B). Simultaneous stimulation induced even stronger cell proliferation (mitotic index: 2.69 ± 0.13) than individual stimulation (Figure 4B). $CD19^+$ B cells were separated into naive (IgD^+CD27^-) and memory ($CD27^+$) cells, and their cell proliferation was compared. Stimulation with αhRP105 showed higher cell proliferation compared to CpGDNA (ΔOD490–630; naive: 0.224 ± 0.0285 vs. 0.160 ± 0.00947, $p < 0.01$; memory: 0.454 ± 0.0918 vs. 0.363 ± 0.0730, $p = 0.168$) (see Figure S7A). Simultaneous stimulation induced even stronger cell proliferation (ΔOD490–630; naive: 0.636 ± 0.0372; memory: 0.626 ± 0.0564) compared to individual stimulation (see Figure S7A). Although αhRP105 and CpGDNA individually led to an increase in activation marker positive cells during B cell proliferation (CD38: 78.3% ± 6.2% vs. 52.7% ± 12.3%, $p < 0.05$; CD80: 60.5% ± 7.6% vs. 40.6% ± 4.4%, $p < 0.05$), simultaneous stimulation resulted in more robust expression of these marker positive cells (CD38: 90.7% ± 2.3% $p < 0.01$, CD80: 76.8% ± 9.9%, $p < 0.01$) (Figures 4C and 4D). Both CD38 (see Figure S7B) and CD80 (see Figure S7C) were also increased in naive and memory B cells upon single stimulation with αhRP105 compared to control (naive: CD38: 61.7% ± 2.61% vs. 28.6% ± 1.02%, CD80: 34.6% ± 2.97% vs. 17.7% ± 3.19%, memory: CD38: 66.3% ± 6.40% vs. 35.5% ± 0.283%, CD80: 36.9% ± 4.67% vs. 18.6% ± 1.21%), and were highly expressed upon simultaneous stimulation, regardless of B cell phenotype (naive: CD38: 75.8% ± 0.651%, CD80: 58.8% ± 3.70%, memory: CD38: 78.7% ± 3.40%, CD80: 49.9% ± 5.98%). These findings indicate that αhRP105 activates both naive and memory B cells, with even stronger activation observed when co-stimulated with CpGDNA. Changes in the behavior of $CD19^+$ B cells with each stimulus were evident, as shown by clear alterations in each cell subtype (see Figure S8). αhRP105 and CpGDNA stimulation increased the frequency of unswitched memory B cells and double-negative B cells, respectively (Figure 4E). However, simultaneous stimulation with αhRP105 and CpGDNA consistently induced the proliferation of switched memory cells in all samples (Figure 4E). We also examined several B cell-related genes. The expression of B cell CLL/lymphoma 6 (BCL6), tumor necrosis factor receptor superfamily member 13c (TNFRSF13C: BAFF-R), and tumor necrosis factor receptor superfamily member 13b (TNFRSF13B: TACI) positive cells was increased in αhRP105-stimulated cells (see Figure S9). Moreover, we compared the expression of the genes induced by αhRP105 and CpGDNA using qRT-PCR. We observed that PR domain zinc finger protein 1 (PRDM1: Blimp-1), a driver gene for B cell differentiation, was not upregulated by αhRP105, but by CpGDNA (Figure 5A). However, glyceraldehyde-3-phosphate dehydrogenase (GAPDH) (Figure 5B) and CCAAT/enhancer-binding protein gamma (CEBPG: C/EBPγ) (Figure 5C) were predominantly upregulated upon αhRP105 stimulation. GAPDH is a glycolytic enzyme that plays important roles in energy production and acts as a sensor of cellular stress.[32] C/EBPγ is a transcription factor that binds to the promoter and enhancer of the immunoglobulin heavy chain and IL-6, which were also upregulated.[33,34] Recent report on C/EBPγ demonstrates its involvement in major physiological processes like controlling of cellular proliferation and inducing of the integrated stress response.[35] Therefore, αhRP105 may induce stress sensor genes.

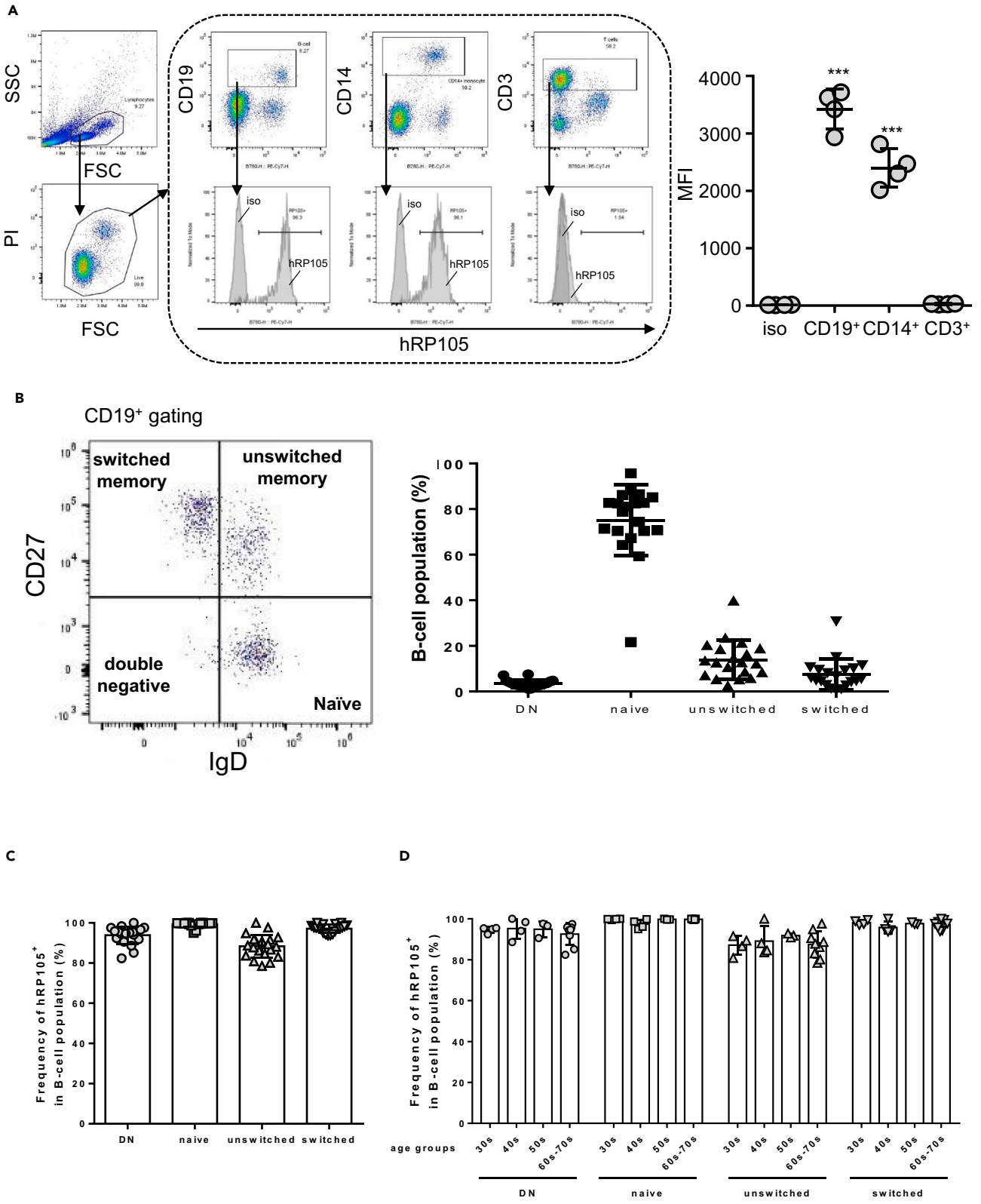
A
SSC
FSC
PI
FSC
CD19
CD14
CD3
iso
hRP105
hRP105
MFI
4000
3000
2000
1000
0
***
***
iso
CD19+
CD14+
CD3+
B
CD19+ gating
switched memory
unswitched memory
double negative
Naïve
CD27
IgD
B-cell population (%)
100
80
60
40
20
0
DN
naive
unswitched
switched
C
Frequency of hRP105+ in B-cell population (%)
100
80
60
40
20
0
DN
naive
unswitched
switched
D
Frequency of hRP105+ in B-cell population (%)
age groups
30s
40s
50s
60s-70s
DN
naive
unswitched
switched

Figure 3. The evaluation of hRP105 expression in human B cells subsets

(A) A representative FCM gating strategy was shown how to evaluate the expression of hRP105 in $CD19^+$ B cells, $CD14^+$ monocyte cells, and $CD3^+$ T cells on the left. The median fluorescence intensity (M.F.I.) of hRP105 on $CD19^+$ B cells, $CD14^+$ monocyte cells, and $CD3^+$ T cells were shown on the right ($n = 4$). "iso" means IgG isotype control. $^{***}p < 0.001$.

(B) Human $CD19^+$ B cells were classified based on CD27 and IgD expression (switched memory; $CD27^+IgD^-$, unswitched memory; $CD27^+IgD^+$, double-negative (DN); $CD27^-IgD^-$, naive; $CD27^-IgD^+$). A representative FCM was shown how to classify human $CD19^+$ B cells on the left. The percentage of each B cell subtype in 20 healthy volunteers was shown as a percentage on the right.

(C) Frequency of hRP105 positive in each B cell subtypes from 20 healthy volunteers was shown.

(D) Frequency of hRP105 positive in each B cell by was shown. Data are represented as mean ± SD.

Intracellular protein expression in $CD19^+$ B cells stimulated by αhRP105 and CpGDNA was measured using liquid chromatography / electrospray ionization-tandem mass spectrometry (LC/ESI-MS/MS) analysis. Purified $CD19^+$ B cells were stimulated with αhRP105 and/or CpGDNA for 24h. Principal component analysis-discriminant analysis (PCA-DA) based on LC/ESI-MS/MS revealed that each stimulus depicted a different expression pattern (Figure 5D). Among these proteins, fatty acid synthase (FASN), which catalyzes the synthesis of palmitic acid from acetyl-CoA and malonyl-CoA to long-chain saturated fatty acids, was increased, and dihydrolipoamide S-succinyltransferase component (DLST), a component of the tricarboxylic acid cycle, was decreased by αhRP105 (Figure 5E). LYN, which is a Src family tyrosine kinase and acts downstream of BCR, and ubiquinol-cytochrome C reductase core protein 2 (UQCRC2), which are associated with mitochondrial respiration, were upregulated by CpGDNA but not by αhRP105 (Figure 5E). These results suggest that αhRP105-stimulated human B cells have a different activation pattern from CpGDNA-stimulated B cells.

αhRP105 stimulates antibody production in $CD19^+$ B cells, which is further enhanced by co-stimulation with CpGDNA

To determine whether αhRP105 stimulation enhances antibody production in $CD19^+$ B cells, purified $CD19^+$ B cells were cultured with αhRP105 with or without CpGDNA, and antibody levels in the culture supernatant were quantified. αhRP105 stimulation produces total IgM levels, but not IgG nor IgA (Figure 6A). However, simultaneous stimulation with αhRP105 and CpGDNA resulted in robust production of IgM, IgG, and IgA antibodies (Figure 6A). The IgG subtype analysis revealed a dominance of IgG1 (Figure 6B). The culture supernatant also exhibited abundant IL-6 production (Figure 6C), and simultaneous stimulation with αhRP105 and CpGDNA induced IL-6 production from both naive (IgD^+CD27^-) and memory ($CD27^+$) human B cells (Figure 6D). Single-cell UMAP analysis revealed that αhRP105 stimulation increased the expression of IL6R and IL6ST genes (Figure 2B). To explore the significance of the IL-6/IL-6R signaling pathway, $CD19^+$ B cells were cultured with an anti-IL-6R antibody, and total IgG and IgM titers in the culture supernatant were measured. The anti-IL-6R antibody partially inhibited IgG and IgM production upon αhRP105 and CpGDNA stimulation (Figure 6E). Subsequently, antigen-specific antibody production was investigated. Simultaneous stimulation with αhRP105 and CpGDNA triggered robust production of blood group IgG and IgM antibodies (anti-blood A antibody, Figure 7A; anti-blood B antibody; Figure 7B). Furthermore, simultaneous stimulation elevated levels of the αGal antibody, a naturally occurring antibody found in all humans (Figure 7C), and this specific antibody was predominantly produced by memory B cells (Figure 7D). Finally, $CD19^+$ B cells were isolated and purified from 22 healthy volunteers ($n = 9$: after the second vaccination, $n = 9$: after the third vaccination, and $n = 4$: after the fourth vaccination) who received more than two doses of the mRNA vaccine against SARS-CoV-2 to detect anti-SARS-CoV-2 S1 antibodies in the culture supernatant. In cultures from healthy volunteers more than 4 weeks post-vaccination, individual stimulation with αhRP105 or CpGDNA yielded nearly identical rates of anti-SARS-CoV-2 S1 antibody production, with CpGDNA producing a slightly higher amount of this antibody (Figure 7E). Simultaneous stimulation with αhRP105 and CpGDNA exhibited the highest antibody titers (55.6% after the second vaccination, 88.9% after the third vaccination, and 100% after the fourth vaccination) among our analyzed samples (Figure 7E). These results suggest that efficient activation of human $CD19^+$ B cells by αhRP105 can effectively induce antigen-specific antibody production through an additive effect with CpGDNA.

DISCUSSION

In this study, we confirmed the robust activation of peripheral human $CD19^+$ B cells by αhRP105 alone in the AIM-V medium. The level of activation observed was comparable to that reported in numerous *in vitro* mouse B cell experiments.[21] LC/ESI-MS/MS experiments were conducted to identify key factors, highlighting the significance of transthyretin and haptoglobin for potent human B cell proliferation induced by αhRP105 (Figure 1). Previous studies explored the role of haptoglobin from mouse liver in B cell activation, particularly in haptoglobin-deficient mice where T and B cell maturation is impaired, leading to inhibition of antigen-specific antibody production.[36] Notably, transthyretin binds retinol-binding proteins and retinoic acid in its complexes.[37] Whereas retinoic acid enhances the generation of gut-tropic IgA^+ plasma cells in skin-draining inguinal lymph nodes, thereby increasing antigen-specific IgA in the intestinal lumen and blood.[38] Although direct evidence linking transthyretin to B cell regulation is inconclusive, the presence of these factors likely contributes to the effective activation of human B cells.

This study is the first demonstrate sufficient human B cell proliferation by αhRP105 alone. Previous studies have demonstrated that αhRP105 alone is not able to adequately promote human B cell proliferation.[24,26] Our culture method also allowed the production of αA IgM, αB IgM, and αGal IgG were produced by αhRP105 stimulation, albeit in limited quantities (Figure 7). αhRP105 activated both naive and memory B cells (see Figure S7), and its stimulation did not necessarily induce the differentiation of naive B cells into memory cells. Previous study has shown that αhRP105 increases TLR9 expression, particularly enhancing TLR9 responses in naive B cells.[26] However, our results

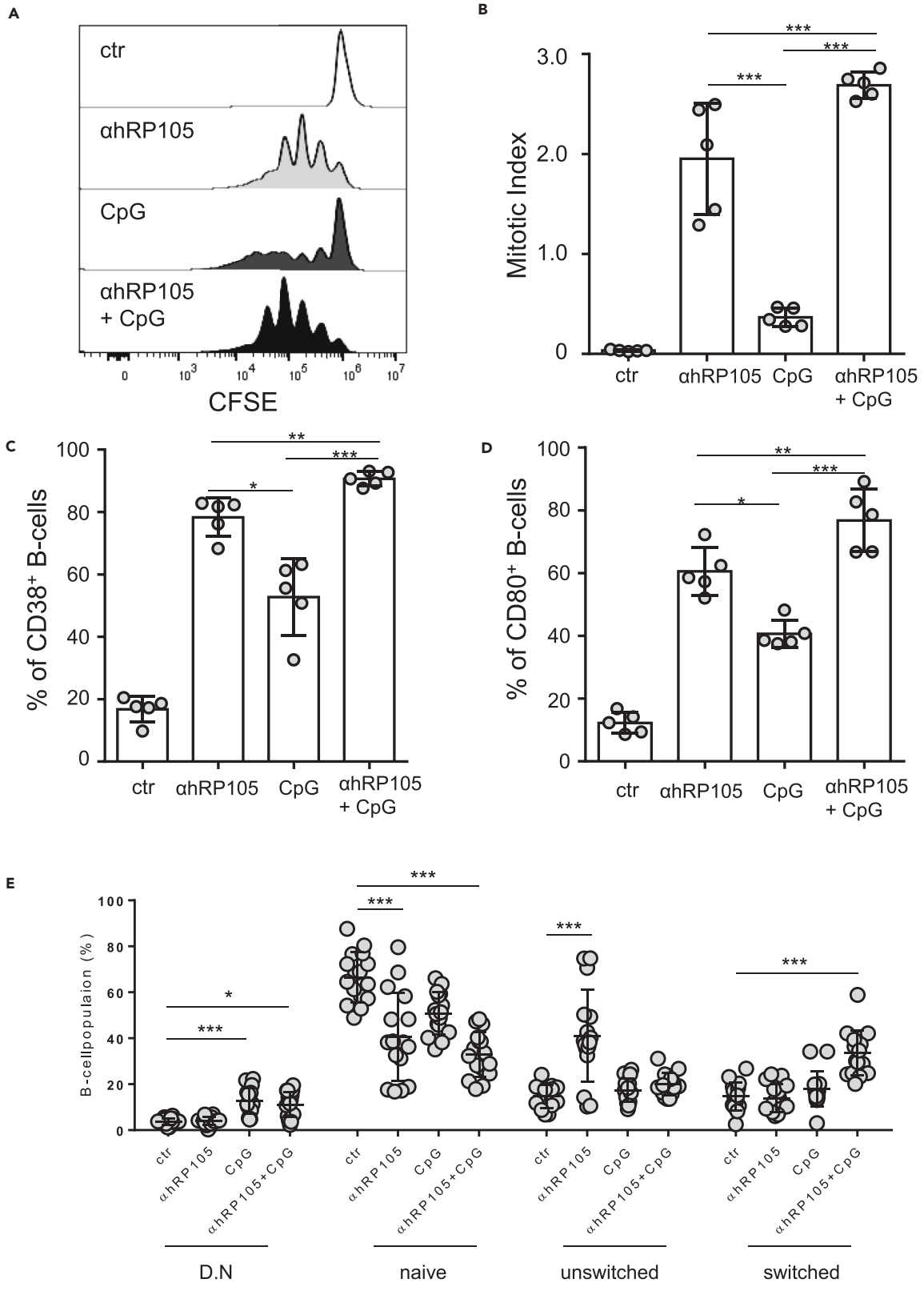
A
ctr
αhRP105
CpG
αhRP105
+ CpG
CFSE
B
Mitotic Index
ctr
αhRP105
CpG
αhRP105
+ CpG
C
% of CD38⁺ B-cells
D
% of CD80⁺ B-cells
E
B-cellpopulaion (%)
D.N
naive
unswitched
switched

Figure 4. Differences between RP105- and TLR9-mediated B cell proliferation and activation

(A) Purified CFSE-stained CD19$^+$ B cells were stimulated with 1.0 μg/mL of αhRP105 and/or CpGDNA, and cultured for 3 days. Representative cell division of CFSE-stained CD19$^+$ B cells was shown.

(B) Purified CD19$^+$ B cells were stimulated with αhRP105 and/or CpGDNA for 3 days. The mitotic index calculated from proliferating CD19$^+$ B cells was shown (n = 5).

(C and D) The expression of CD38 (C) and CD80 (D) activation markers were evaluated by FCM. Each activation marker (CD38 and CD80) positive rate from CD19$^+$ B cells was shown (n = 5).

(E) Purified CD19$^+$ B cells were stimulated with 1.0 μg/mL of αhRP105 and/or CpGDNA and cultured for 3days. CD19$^+$ B cells were classified based on CD27 and IgD expression (double-negative (DN); CD27$^-$IgD$^-$, naive; CD27$^-$IgD$^+$, unswitched memory; CD27$^+$IgD$^+$, switched memory; CD27$^+$IgD$^-$) (n = 16). Representative FCM results were shown in Figure S8. *p < 0.05, **p < 0.01, ***p < 0.001. Data are represented as mean ± SD.

indicated that αhRP105 broadly activated and proliferated B cells subsets, leading to antibody production in coordination with CpGDNA stimulation.

The current results suggested the differences of character between αhRP105 and CpGDNA. αhRP105 significantly promoted cell proliferation (Figure 4) and metabolic systems, whereas CpGDNA was crucial for antibody producing functions (Figures 6 and 7). αhRP105 stimulation

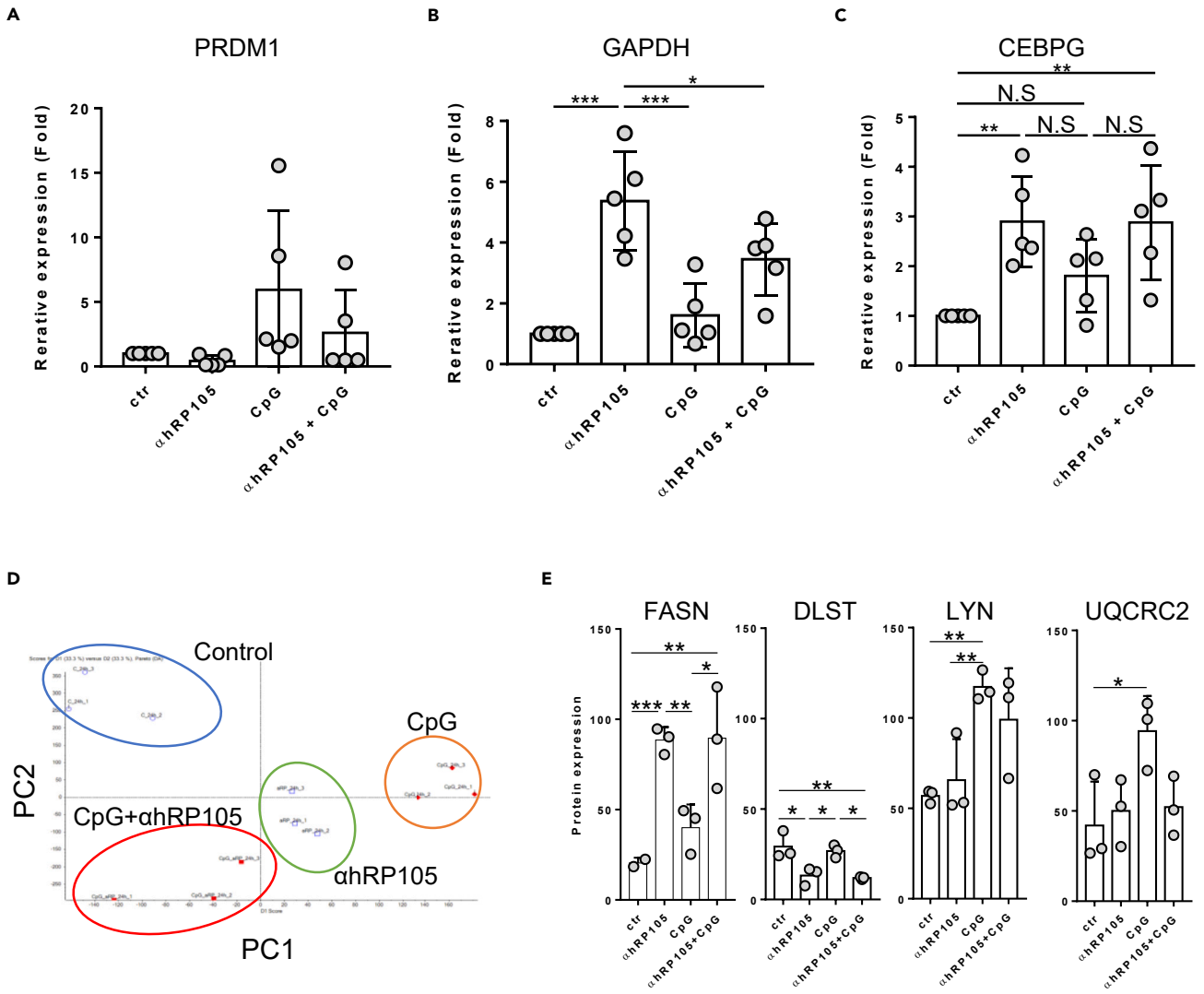

Figure 5. Differences between RP105- and TLR9-mediated gene expression

(A–C) Purified CD19$^+$ B-cells were cultured with 1.0 μg/mL of αhRP105 and/or CpGDNA for 24h (A) and 3days (B and C). The gene expression levels of PRDM1 (A), GAPDH (B), and CEBPG (C) were determined by qRT-PCR. Data were normalized to β-actin (A; TaqMan probe) and 18S rRNA (B, C; SYBR Green) and shown as fold-change compared with control (ctr) (n = 5).

(D and E) LC/ESI-MS/MS analysis was conducted, and the protein expression trends were analyzed using principal component analysis-discriminant analysis in MarkerView Software (D). FASN, DLST, LYN, and UQCRC2, four proteins from LC/ESI-MS/MS analysis that were differentially induced by αhRP105 and CpGDNA stimuli (E) (n = 3). *p < 0.05, **p < 0.01, ***p < 0.001. Data are represented as mean ± SD.

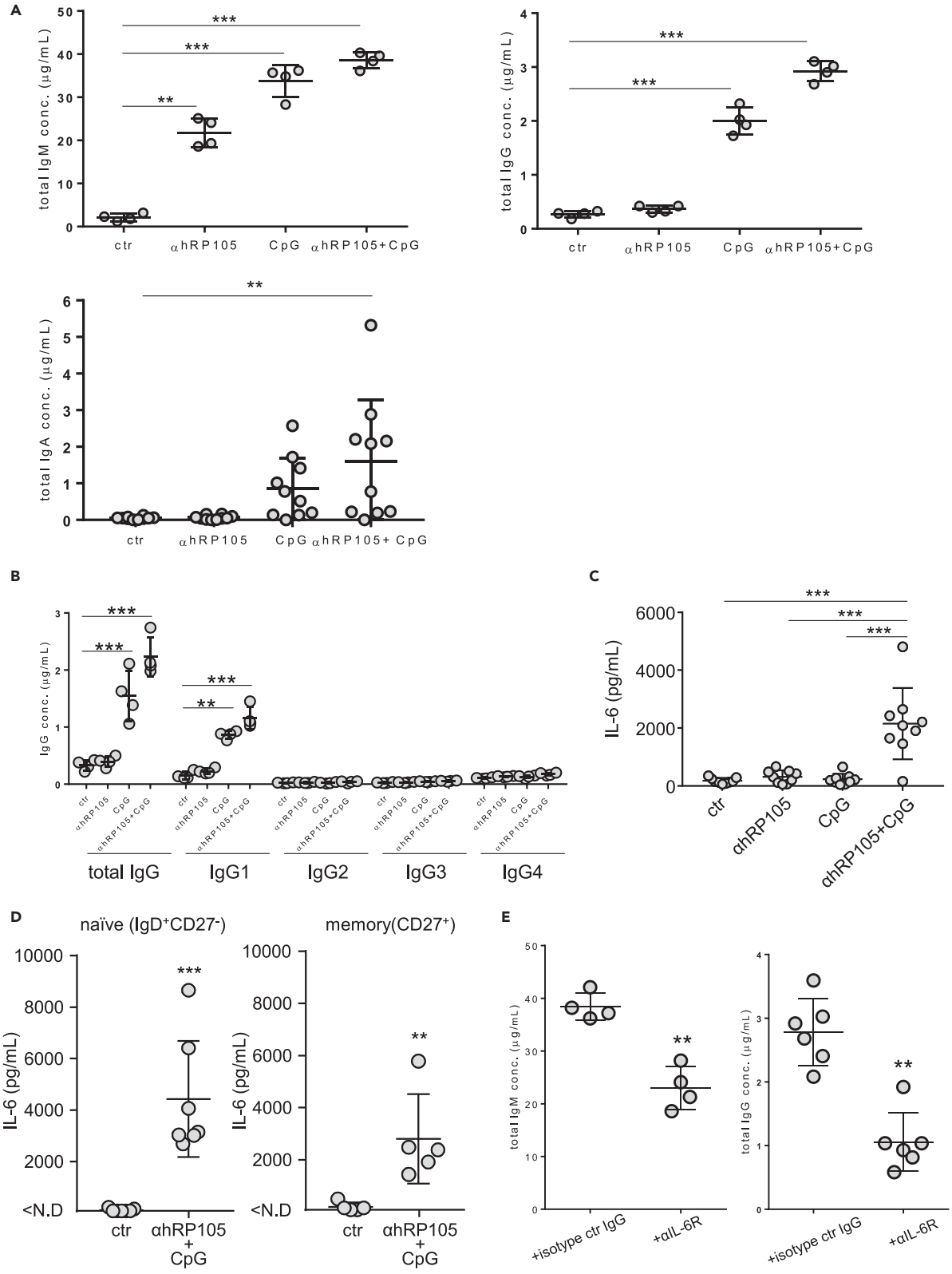
A
total IgM conc. (μg/mL)
ctr
αhRP105
CpG
αhRP105+CpG
total IgG conc. (μg/mL)
total IgA conc. (μg/mL)
B
IgG conc. (μg/mL)
total IgG
IgG1
IgG2
IgG3
IgG4
C
IL-6 (pg/mL)
ctr
dhRP105
CpG
dhRP105+CpG
D
naïve (IgD+CD27-)
memory(CD27+)
IL-6 (pg/mL)
<N.D
ctr
αhRP105 + CpG
E
total IgM conc. (μg/mL)
total IgG conc. (μg/mL)
+isotype ctr IgG
+αIL-6R

Figure 6. The increment of antibody production and IL-6 cytokine from CD19$^+$ B-cells stimulated with αhRP105 and CpGDNA

(A–C) Purified CD19$^+$ B cells were cultured for 10 days with 1.0 μg/mL of αhRP105 or CpGDNA individually, or with simultaneous stimulation. Total IgM (A, left), IgG (A, right), IgA (A, bottom), IgG subtype (B), and IL-6 (C) in culture supernatants were measured by ELISA (A [total IgM and total IgG]: $n = 4$, A [total IgA]: $n = 10$, B: $n = 4$, C: $n = 9$).

(D) Purified naive (IgD$^+$CD27$^-$) and memory (CD27$^+$) B-cells from healthy volunteers were cultured for 2days with 1.0 μg/mL of αhRP105 and CpGDNA with simultaneous stimulation. IL-6 in the culture supernatants were measured by ELISA (naive: $n = 7$, memory: $n = 5$).

(E) Purified CD19$^+$ B cells were stimulated with 1.0 μg/mL αhRP105 and CpGDNA in the presence of isotype control anti-rabbit IgG (+isotype ctr IgG) or anti-IL-6R (+αIL-6R) for 10days. Total IgM (left) and IgG (right) in culture supernatants were measured by ELISA (IgM: $n = 4$, IgG: $n = 6$). $^{**}p < 0.01$, $^{***}p < 0.01$. Data are represented as mean ± SD.

upregulated the metabolic protein FASN compared to CpGDNA. Inhibition of FASN has been reported to promote cell death in a Bcl2-dependent manner,[39,40] and its induction may correlate with cell proliferation. Conversely, CpGDNA increased the expression of LYN. This observation is supported by the upregulation of stress-sensor genes, GAPDH[41] and CEBPG,[35] upon αhRP105 stimulation, and the upregulation of Blimp-1, a driver gene for B cell differentiation,[42] by CpGDNA but not αhRP105 (Figure 5). Additionally, heightened expression of IL-6 (Figure 6) and CD44 (see Figure S10) was detected only upon simultaneous stimulation with αhRP105 and CpGDNA in B cells, correlating with specific antibody production. CD44, a transmembrane glycoprotein receptor for hyaluronan, plays crucial roles in cell-cell interactions,[43] and has implications in B cell malignancies, potentially contributing to B cell proliferation upon co-stimulation.[44]

In clinical situations, our current culture method could be applied in two ways. First, it could enhance the detection of donor human leukocyte antigen specific antibody (DSA) in organ transplantation[45] and autoantibodies in autoimmune diseases,[46] which cause tissue injury. This stable B cell culture method can improve the sensitivity of detecting DSAs and autoantibodies that may not be detectable in peripheral blood alone. Moreover, it may contribute to the analysis of disease-associated antibody-producing B cell/BCR repertoires and relevant immune responses such as follicular helper T cell/T cell receptor repertoires, thereby enabling more effective therapeutic strategies. Our method may also be used therapeutically for *ex vivo* expansion of B cells. Given the widespread use of mRNA vaccines against SARS-CoV-2 during the pandemic,[16] addressing the challenges of low antibody acquisition in organ transplant recipients and autoimmune disease patients undergoing immunosuppressive therapy, as well as in immunodeficient patients such as those with CVID, remains critical. CVID is a disease characterized by low levels of serum immunoglobulins, resulting in a high incidence of infections.[25] Patients with CVID typically have reduced numbers of memory B cells whereas maintaining normal levels of naive B cells, which can be activated through RP105.[25] A potential therapeutic strategy could involve purifying B cells from such individuals, generating *ex vivo* immunoglobulin-producing B cells, such as specific antibodies against SARS-CoV-2, and reintroducing them into the patients. Furthermore, adjuvant use of αhRP105 in vaccination should also be considered in future.

Limitations of the study

The hRP105 molecule is expressed on both B cells and CD14$^+$ monocytes (Figure 3). Understanding the role of hRP105 in the monocyte lineage is crucial for its practical clinical use. Moreover, using CD19 as a marker to purify B cells for antibody production presents challenges since human plasma cells typically do not express CD19. Notably, the proportion of plasma cells in the peripheral blood is extremely low, as they are typically found in the spleen and bone marrow. Antibody-producing B cells should be present in the body because all subjects' serum produces antibodies against SARS-CoV-2 S1 (see Figure S11). Collecting blood samples from the human spleen or bone marrow presented challenges because of the limited amount of blood collected. Consequently, confirming the presence of B cells that produce anti-SARS-CoV-2 S1 antibodies across all samples was difficult.

STAR★METHODS

Detailed methods are provided in the online version of this paper and include the following:

- KEY RESOURCES TABLE
- RESOURCE AVAILABILITY
  - Lead contact
  - Materials availability
  - Data and code availability
- EXPERIMENTAL MODEL AND STUDY PARTICIPANT DETAILS
  - Human subjects
- METHOD DETAILS
  - *In vitro* B-cell proliferation assay (carboxyfluorescein diacetate, succinimidyl ester (CFSE)-based cell proliferation assay)
  - *In vitro* naive (IgD$^+$CD27$^-$) and memory (CD27$^+$) B-cells proliferation assay (MTS-based cell viability assay)
  - *In vitro* cluster formation of B-cells
  - LC/ESI-MS/MS and DDA-MS data analysis
  - Zeno SWATH-MS data acquisition
  - Single-cell RNA library construction and sequencing
  - Measurement of hRP105 expression on human B-cells

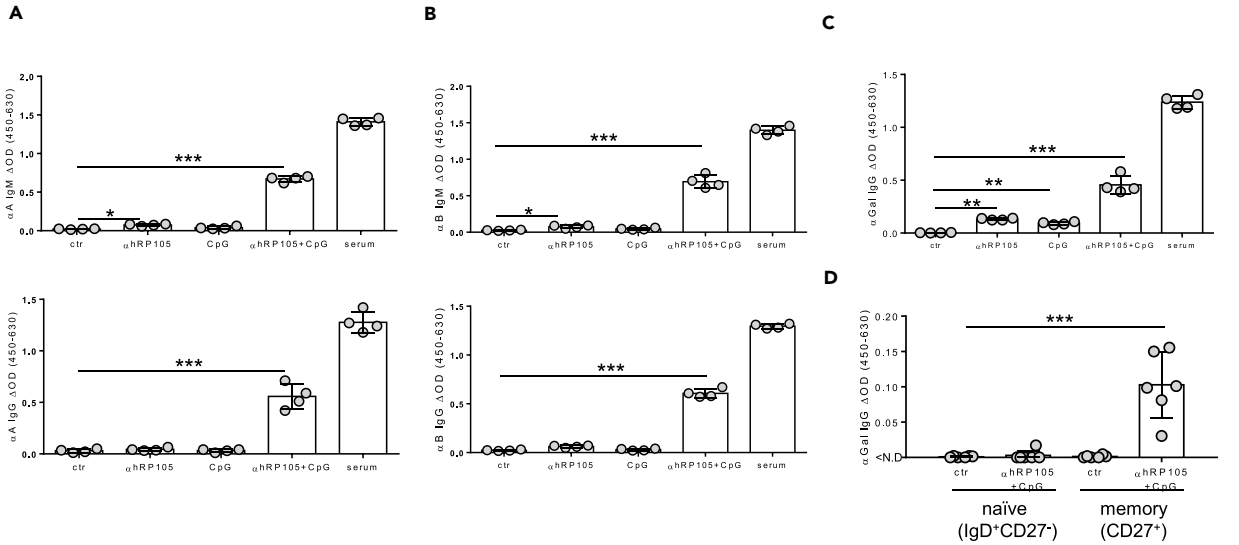
A
B
C
D
ctr
αhRP105
CpG
αhRP105+CpG
serum
naïve
(IgD+CD27-)
memory
(CD27+)

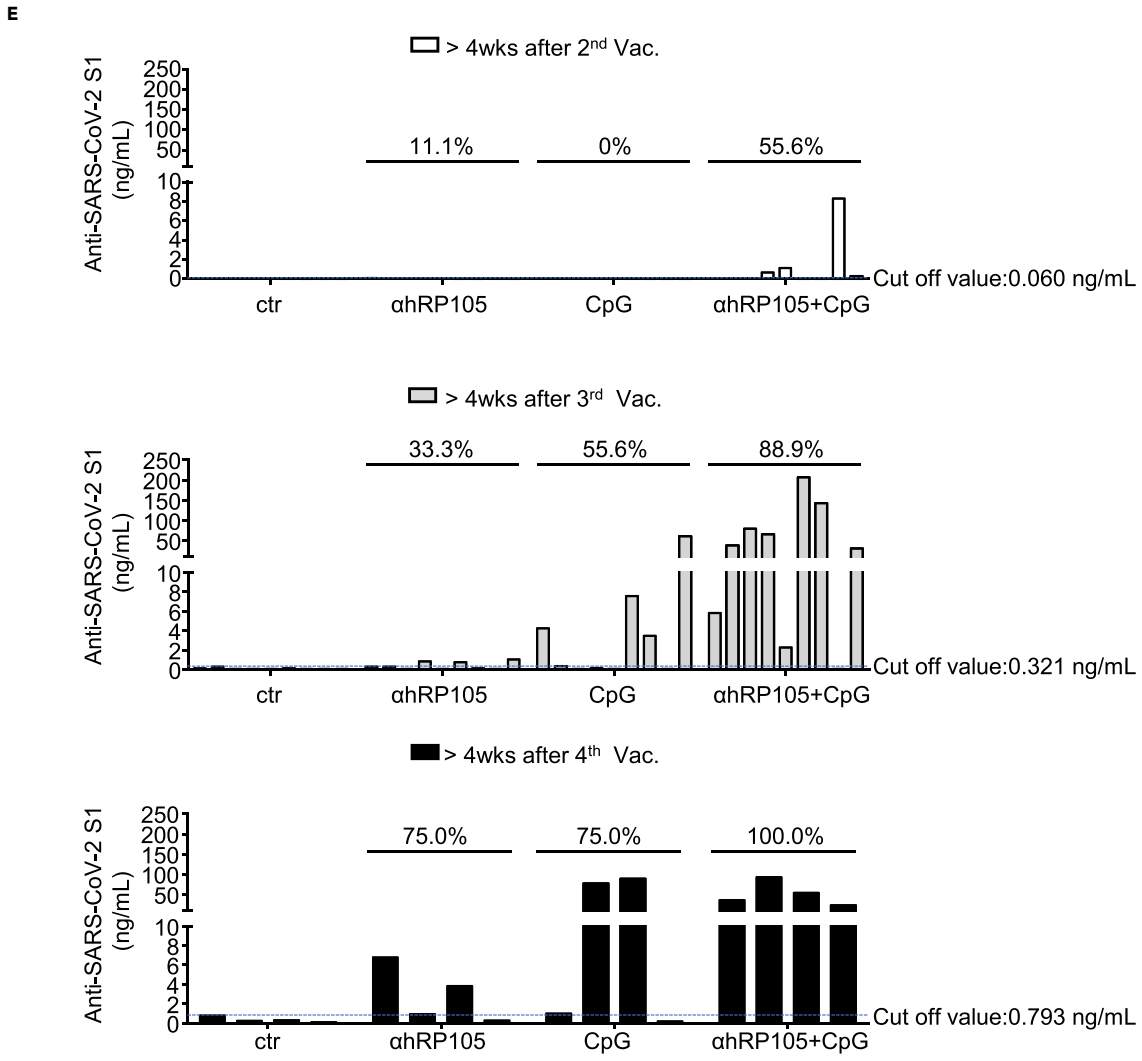
E
> 4wks after 2nd Vac.
11.1%
0%
55.6%
Cut off value:0.060 ng/mL
> 4wks after 3rd Vac.
33.3%
55.6%
88.9%
Cut off value:0.321 ng/mL
> 4wks after 4th Vac.
75.0%
75.0%
100.0%
Cut off value:0.793 ng/mL
Anti-SARS-CoV-2 S1 (ng/mL)
ctr
αhRP105
CpG
αhRP105+CpG

Figure 7. The antigen-specific antibody production from CD19$^+$ B cells stimulated with αhRP105 and CpGDNA

(A–C) Purified CD19$^+$ B cells from healthy volunteers were cultured for 10 days with 1.0 μg/mL of αhRP105 or CpGDNA individually, or with simultaneous stimulation. Anti-blood A IgM (A, top) and IgG (A, bottom) antibodies, anti-blood B IgM (B, top) and IgG (B, bottom) antibodies, and anti-αGal IgG antibodies (C) in culture supernatants were measured by ELISA (n = 4).

(D) naive (IgD$^+$CD27$^-$) and memory (CD27$^+$) B cells were purified from healthy volunteers and cultured for 10 days with 1.0 μg/mL of αhRP105 and CpGDNA. Anti-αGal antibodies in culture supernatants were measured by ELISA (n = 6).

(E) Purified CD19$^+$ B cells from healthy volunteers who had more than two-dose regimen of either the Moderna (mRNA-1273) or Pfizer-BioNTech (BNT162b2) mRNA vaccine were cultured for 10 days with 1.0 μg/mL of αhRP105 or CpGDNA individually, or with simultaneous stimulation. Anti-SARS-CoV-2 S1 antibodies in culture supernatants were measured by ELISA (second vaccination: n = 9, third vaccination: n = 9, and fourth vaccination: n = 4). As for the measurement of anti-SARS-CoV-2 S1 antibodies, the graphs are shown for each vaccination frequency. The respective cut-off values are determined with the highest level of anti-SARS-CoV-2 S1 antibodies in ctr. The numbers (%) above each group represent the positive ratio determined by the cut-off value. Data are represented as mean ± SD.

- Quantitative real-time PCR (qRT-PCR)
- *In vitro* antibody production from CD19$^+$ B-cells stimulated with αhRP105 and CpGDNA
- Enzyme-linked immunosorbent assay (ELISA)
- Statistical analysis

SUPPLEMENTAL INFORMATION

Supplemental information can be found online at https://doi.org/10.1016/j.isci.2024.110649.

ACKNOWLEDGMENTS

The authors would like to have special thanks to lab members for their contribution to this study. The authors would like to also thank the Aichi Medical University Comprehensive Medical Research Organization for their cooperation. The authors would also like to thank MARUZEN-YUSHODO Co., Ltd. (https://kw.maruzen.co.jp/kousei-honyaku/) for the English language editing.

Funding: This work was partly supported by KAKENHI grant numbers JP21K09385, JP15K15472, JP19K08500, and JP16H05465 from the Japan Society for the Promotion of Science and supported by Aichi Medical University Research unit grant aid. This study was also supported partly by a grant from International Joint Usage/Research Center, the Institute of Medical Science, the University of Tokyo (ID no. 22-3064).

AUTHOR CONTRIBUTIONS

T.Y., K.I., and S.A.-T. designed the research and T.Y., K.I., M.I., D.O., and S.A.-T. wrote the paper. T.Y., K.I., and S.T. performed the research under the supervision of S.A.-T., K.I., and D.O. conducted scRNA-seq, and M.I. analyzed sequence date by Seurat. S.T. performed and analyzed liquid chromatography with tandem massspectrometry (LC-MS/MS). T.Y., K.I., S.T., M.I., Y.M., M.I., T.K., and S.A.-T. participate in the data analysis.; Y.M., M.S., S.A., K.I., M.O., and T.K. manage kidney transplant patients and collect blood samples from those patients.

DECLARATION OF INTERESTS

The authors declare no conflicts of interest associated with this manuscript.

Received: February 9, 2024
Revised: May 16, 2024
Accepted: July 31, 2024
Published: August 3, 2024

REFERENCES

1. Schultz, T.E., and Blumenthal, A. (2017). The RP105/MD-1 complex: molecular signaling mechanisms and pathophysiological implications. J. Leukoc. Biol. *101*, 183–192. https://doi.org/10.1189/jlb.2VMR1215-582R.
2. Dunne, A., and O'Neill, L.A.J. (2003). The interleukin-1 receptor/Toll-like receptor superfamily: signal transduction during inflammation and host defense. Sci. STKE *2003*, re3. https://doi.org/10.1126/stke.2003.171.re3.
3. Miyake, K., Yamashita, Y., Hitoshi, Y., Takatsu, K., and Kimoto, M. (1994). Murine B cell proliferation and protection from apoptosis with an antibody against a 105-kD molecule: unresponsiveness of X-linked immunodeficient B cells. J. Exp. Med. *180*, 1217–1224. https://doi.org/10.1084/jem.180.4.1217.
4. Erdő-Bonyár, S., Rapp, J., Minier, T., Ráth, G., Najbauer, J., Czirják, L., Németh, P., Berki, T., and Simon, D. (2019). Toll-Like Receptor Mediated Activation of Natural Autoantibody Producing B Cell Subpopulations in an Autoimmune Disease Model. Int. J. Mol. Sci. *20*, 6152. https://doi.org/10.3390/ijms20246152.
5. Nagai, Y., Shimazu, R., Ogata, H., Akashi, S., Sudo, K., Yamasaki, H., Hayashi, S.I., Iwakura, Y., Kimoto, M., and Miyake, K. (2002). Requirement for MD-1 in cell surface expression of RP105/CD180 and B-cell responsiveness to lipopolysaccharide. Blood *99*, 1699–1705. https://doi.org/10.1182/blood.v99.5.1699.
6. Miyake, K., Shimazu, R., Kondo, J., Niki, T., Akashi, S., Ogata, H., Yamashita, Y., Miura, Y., and Kimoto, M. (1998). Mouse MD-1, a molecule that is physically associated with RP105 and positively regulates its expression. J. Immunol. *161*, 1348–1353.
7. Biswas, M., Yamazaki, T., Tomono, S., Karnan, S., Takagi, H., Ichimonji, I., Inui, M., Nagaoka, F., Hosokawa, Y., and Akashi-Takamura, S. (2022). Cell surface expression of human RP105 depends on N-glycosylation of MD-1. FEBS Lett. *596*, 3211–3231. https://doi.org/10.1002/1873-3468.14452.

8. Gilljam, K.M., Holm, K.L., Zahoor, M., Centonze, F.G., Farhan, H., and Blomhoff, H.K. (2020). Differential Effects of Reactive Oxygen Species on IgG versus IgM Levels in TLR-Stimulated B Cells. J. Immunol. *204*, 2133–2142. https://doi.org/10.4049/jimmunol.1901131.
9. Theofilopoulos, A.N., and Dixon, F.J. (1985). Murine models of systemic lupus erythematosus. Adv. Immunol. *37*, 269–390. https://doi.org/10.1016/s0065-2776(08)60342-9.
10. Fujita, K., Akasaka, Y., Kuwabara, T., Wang, B., Tanaka, K., Kamata, I., Yokoo, T., Kinoshita, T., Iuchi, A., Akishima-Fukasawa, Y., et al. (2012). Pathogenesis of lupus-like nephritis through autoimmune antibody produced by CD180-negative B lymphocytes in NZBWF1 mouse. Immunol. Lett. *144*, 1–6. https://doi.org/10.1016/j.imlet.2012.02.012.
11. Kikuchi, Y., Koarada, S., Tada, Y., Ushiyama, O., Morito, F., Suzuki, N., Ohta, A., Miyake, K., Kimoto, M., Horiuchi, T., and Nagasawa, K. (2002). RP105-lacking B cells from lupus patients are responsible for the production of immunoglobulins and autoantibodies. Arthritis Rheum. *46*, 3259–3265. https://doi.org/10.1002/art.10672.
12. Koarada, S., Tada, Y., Suematsu, R., Soejima, S., Inoue, H., Ohta, A., and Nagasawa, K. (2012). Phenotyping of P105-negative B cell subsets in patients with systemic lupus erythematosus. Clin. Dev. Immunol. *2012*, 198206. https://doi.org/10.1155/2012/198206.
13. Koarada, S., Tashiro, S., Nagao, N., Suematsu, R., Ohta, A., and Tada, Y. (2013). Increased RP105-Negative B Cells in IgG4-Related Disease. Open Rheumatol. J. *7*, 55–57. https://doi.org/10.2174/1874312901307010055.
14. Yamazaki, T., Biswas, M., Kosugi, K., Nagashima, M., Inui, M., Tomono, S., Takagi, H., Ichimonji, I., Nagaoka, F., Ainai, A., et al. (2020). A Novel Gene Delivery Vector of Agonistic Anti-Radioprotective 105 Expressed on Cell Membranes Shows Adjuvant Effect for DNA Immunization Against Influenza. Front. Immunol. *11*, 606518. https://doi.org/10.3389/fimmu.2020.606518.
15. Tauzin, A., Gong, S.Y., Beaudoin-Bussières, G., Vézina, D., Gasser, R., Nault, L., Marchitto, L., Benlarbi, M., Chatterjee, D., Nayrac, M., et al. (2022). Strong humoral immune responses against SARS-CoV-2 Spike after BNT162b2 mRNA vaccination with a 16-week interval between doses. Cell Host Microbe *30*, 97–109.e105. https://doi.org/10.1016/j.chom.2021.12.004.
16. Dejnirattisai, W., Huo, J., Zhou, D., Zahradník, J., Supasa, P., Liu, C., Duyvesteyn, H.M.E., Ginn, H.M., Mentzer, A.J., Tuekprakhon, A., et al. (2022). SARS-CoV-2 Omicron-B.1.1.529 leads to widespread escape from neutralizing antibody responses. Cell *185*, 467–484.e15. https://doi.org/10.1016/j.cell.2021.12.046.
17. Cucchiari, D., Egri, N., Bodro, M., Herrera, S., Del Risco-Zevallos, J., Casals-Urquiza, J., Cofan, F., Moreno, A., Rovira, J., Banon-Maneus, E., et al. (2021). Cellular and humoral response after MRNA-1273 SARS-CoV-2 vaccine in kidney transplant recipients. Am. J. Transplant. *21*, 2727–2739. https://doi.org/10.1111/ajt.16701.
18. Kamar, N., Abravanel, F., Marion, O., Couat, C., Izopet, J., and Del Bello, A. (2021). Three Doses of an mRNA Covid-19 Vaccine in Solid-Organ Transplant Recipients. N. Engl. J. Med. *385*, 661–662. https://doi.org/10.1056/NEJMc2108861.
19. Achiron, A., Mandel, M., Dreyer-Alster, S., Harari, G., Dolev, M., Menascu, S., Magalashvili, D., Flechter, S., Givon, U., Guber, D., et al. (2021). Humoral immune response in multiple sclerosis patients following PfizerBNT162b2 COVID19 vaccination: Up to 6 months cross-sectional study. J. Neuroimmunol. *361*, 577746. https://doi.org/10.1016/j.jneuroim.2021.577746.
20. Sicard, T., Kassardjian, A., and Julien, J.P. (2020). B cell targeting by molecular adjuvants for enhanced immunogenicity. Expert Rev. Vaccines *19*, 1023–1039. https://doi.org/10.1080/14760584.2020.1857736.
21. Chaplin, J.W., Kasahara, S., Clark, E.A., and Ledbetter, J.A. (2011). Anti-CD180 (RP105) activates B cells to rapidly produce polyclonal Ig via a T cell and MyD88-independent pathway. J. Immunol. *187*, 4199–4209. https://doi.org/10.4049/jimmunol.1100198.
22. Chaplin, J.W., Chappell, C.P., and Clark, E.A. (2013). Targeting antigens to CD180 rapidly induces antigen-specific IgG, affinity maturation, and immunological memory. J. Exp. Med. *210*, 2135–2146. https://doi.org/10.1084/jem.20130188.
23. Miura, Y., Shimazu, R., Miyake, K., Akashi, S., Ogata, H., Yamashita, Y., Narisawa, Y., and Kimoto, M. (1998). RP105 is associated with MD-1 and transmits an activation signal in human B cells. Blood *92*, 2815–2822.
24. Eriksen, A.B., Indrevær, R.L., Holm, K.L., Landskron, J., and Blomhoff, H.K. (2012). TLR9-signaling is required for turning retinoic acid into a potent stimulator of RP105 (CD180)-mediated proliferation and IgG synthesis in human memory B cells. Cell. Immunol. *279*, 87–95. https://doi.org/10.1016/j.cellimm.2012.09.003.
25. Indrevær, R.L., Holm, K.L., Aukrust, P., Osnes, L.T., Naderi, E.H., Fevang, B., and Blomhoff, H.K. (2013). Retinoic acid improves defective TLR9/RP105-induced immune responses in common variable immunodeficiency-derived B cells. J. Immunol. *191*, 3624–3633. https://doi.org/10.4049/jimmunol.1300213.
26. Yamazaki, K., Yamazaki, T., Taki, S., Miyake, K., Hayashi, T., Ochs, H.D., and Agematsu, K. (2010). Potentiation of TLR9 responses for human naïve B-cell growth through RP105 signaling. Clin. Immunol. *135*, 125–136. https://doi.org/10.1016/j.clim.2009.12.013.
27. Haniuda, K., and Kitamura, D. (2019). Induced Germinal Center B Cell Culture System. Bio. Protoc. *9*, e3163. https://doi.org/10.21769/BioProtoc.3163.
28. Goel, R.R., Painter, M.M., Apostolidis, S.A., Mathew, D., Meng, W., Rosenfeld, A.M., Lundgreen, K.A., Reynaldi, A., Khoury, D.S., Pattekar, A., et al. (2021). mRNA vaccines induce durable immune memory to SARS-CoV-2 and variants of concern. Science *374*, abm0829. https://doi.org/10.1126/science.abm0829.
29. Haneda, M., Owaki, M., Kuzuya, T., Iwasaki, K., Miwa, Y., and Kobayashi, T. (2014). Comparative analysis of drug action on B-cell proliferation and differentiation for mycophenolic acid, everolimus, and prednisolone. Transplantation *97*, 405–412. https://doi.org/10.1097/01.TP.0000441826.70687.f6.
30. Helinski, E.H., Bielat, K.L., Ovak, G.M., and Pauly, J.L. (1988). Long-term cultivation of functional human macrophages in Teflon dishes with serum-free media. J. Leukoc. Biol. *44*, 111–121. https://doi.org/10.1002/jlb.44.2.111.
31. Martin, V.G., Wu, Y.C.B., Townsend, C.L., Lu, G.H.C., O'Hare, J.S., Mozeika, A., Coolen, A.C.C., Kipling, D., Fraternali, F., and Dunn-Walters, D.K. (2016). Transitional B Cells in Early Human B Cell Development - Time to Revisit the Paradigm? Front. Immunol. *7*, 546. https://doi.org/10.3389/fimmu.2016.00546.
32. Tristan, C., Shahani, N., Sedlak, T.W., and Sawa, A. (2011). The diverse functions of GAPDH: views from different subcellular compartments. Cell. Signal. *23*, 317–323. https://doi.org/10.1016/j.cellsig.2010.08.003.
33. Roman, C., Platero, J.S., Shuman, J., and Calame, K. (1990). Ig/EBP-1: a ubiquitously expressed immunoglobulin enhancer binding protein that is similar to C/EBP and heterodimerizes with C/EBP. Genes Dev. *4*, 1404–1415. https://doi.org/10.1101/gad.4.8.1404.
34. Gao, H., Parkin, S., Johnson, P.F., and Schwartz, R.C. (2002). C/EBP gamma has a stimulatory role on the IL-6 and IL-8 promoters. J. Biol. Chem. *277*, 38827–38837. https://doi.org/10.1074/jbc.M206224200.
35. Renfro, Z., White, B.E., and Stephens, K.E. (2022). CCAAT enhancer binding protein gamma (C/EBP-γ): An understudied transcription factor. Adv. Biol. Regul. *84*, 100861. https://doi.org/10.1016/j.jbior.2022.100861.
36. Huntoon, K.M., Russell, L., Tracy, E., Barbour, K.W., Li, Q., Shrikant, P.A., Berger, F.G., Garrett-Sinha, L.A., and Baumann, H. (2013). A unique form of haptoglobin produced by murine hematopoietic cells supports B-cell survival, differentiation and immune response. Mol. Immunol. *55*, 345–354. https://doi.org/10.1016/j.molimm.2013.03.008.
37. Horwitz, J., and Heller, J. (1973). Interactions of all-trans, 9-11-and 13-cis-retinal, all-trans-retinyl acetate, and retinoic acid with human retinol-binding protein and prealbumin. J. Biol. Chem. *248*, 6317–6324.
38. Hammerschmidt, S.I., Friedrichsen, M., Boelter, J., Lyszkiewicz, M., Kremmer, E., Pabst, O., and Förster, R. (2011). Retinoic acid induces homing of protective T and B cells to the gut after subcutaneous immunization in mice. J. Clin. Invest. *121*, 3051–3061. https://doi.org/10.1172/JCI44262.
39. Xu, M., Ding, L., Liang, J., Yang, X., Liu, Y., Wang, Y., Ding, M., and Huang, X. (2021). NAD kinase sustains lipogenesis and mitochondrial metabolismthrough fatty acid synthesis. Cell Rep. *37*, 110157. https://doi.org/10.1016/j.celrep.2021.110157.
40. Schroeder, B., Vander Steen, T., Espinoza, I., Venkatapoorna, C.M.K., Hu, Z., Silva, F.M., Regan, K., Cuyàs, E., Meng, X.W., Verdura, S., et al. (2021). Fatty acid synthase (FASN) regulates the mitochondrial priming of cancer cells. Cell Death Dis. *12*, 977. https://doi.org/10.1038/s41419-021-04262-x.
41. Hildebrandt, T., Knuesting, J., Berndt, C., Morgan, B., and Scheibe, R. (2015). Cytosolic thiol switches regulating basic cellular functions: GAPDH as an information hub? Biol. Chem. *396*, 523–537. https://doi.org/10.1515/hsz-2014-0295.
42. Robinson, E., Care, M.A., Walker, K., Campbell, M., Tooze, R.M., and Doody, G.M. (2022). A System for In Vitro Generation of Mature Murine Plasma Cells Uncovers Differential. J. Immunol. *208*, 514–525. https://doi.org/10.4049/jimmunol.2100004.

43. Yan, Y., Zuo, X., and Wei, D. (2015). Concise Review: Emerging Role of CD44 in Cancer Stem Cells: A Promising Biomarker and Therapeutic Target. Stem Cells Transl. Med. *4*, 1033–1043. https://doi.org/10.5966/sctm.2015-0048.
44. Burger, J.A., Sivina, M., and Ravandi, F. (2011). The microenvironment in hairy cell leukemia: pathways and potential therapeutic targets. Leuk. Lymphoma *52*, 94–98. https://doi.org/10.3109/10428194.2011.568649.
45. Yamamoto, T., Watarai, Y., Takeda, A., Tsujita, M., Hiramitsu, T., Goto, N., Narumi, S., Katayama, A., Morozumi, K., Uchida, K., and Kobayashi, T. (2016). De Novo Anti-HLA DSA Characteristics and Subclinical Antibody-Mediated Kidney Allograft Injury. Transplantation *100*, 2194–2202. https://doi.org/10.1097/TP.0000000000001012.
46. Moroney, J.B., Chupp, D.P., Xu, Z., Zan, H., and Casali, P. (2020). Epigenetics of the antibody and autoantibody response. Curr. Opin. Immunol. *67*, 75–86. https://doi.org/10.1016/j.coi.2020.09.004.
47. Kenta, I., Toshihide, T., Takashi, S., Shintaro, S., Yuko, M., Manabu, O., Takahisa, H., Norihiko, G., Shunji, N., Yoshihiko, W., et al. (2023). Estimation of Sensitization Status in Renal Transplant Recipients by Assessing Indirect Pathway CD4 + T Cell Response to Donor Cell-pulsed Dendritic Cell. Transplantation *107*, 1079–1088. https://doi.org/10.1097/tp.0000000000004491.
48. Demichev, V., Messner, C.B., Vernardis, S.I., Lilley, K.S., and Ralser, M. (2020). DIA-NN: neural networks and interference correction enable deep proteome coverage in high throughput. Nat. Methods *17*, 41–44. https://doi.org/10.1038/s41592-019-0638-x.
49. Hao, Y., Hao, S., Andersen-Nissen, E., Mauck, W.M., Zheng, S., Butler, A., Lee, M.J., Wilk, A.J., Darby, C., Zager, M., et al. (2021). Integrated analysis of multimodal single-cell data. Cell *184*, 3573–3587.e29. https://doi.org/10.1016/j.cell.2021.04.048.
50. Stoeckius, M., Zheng, S., Houck-Loomis, B., Hao, S., Yeung, B.Z., Mauck, W.M., Smibert, P., and Satija, R. (2018). Cell Hashing with barcoded antibodies enables multiplexing and doublet detection for single cell genomics. Genome Biol. *19*, 224. https://doi.org/10.1186/s13059-018-1603-1.
51. Karnan, S., Ota, A., Murakami, H., Rahman, M.L., Wahiduzzaman, M., Hasan, M.N., Vu, L.Q., Hanamura, I., Inoko, A., Riku, M., et al. (2023). CAMK2D: a novel molecular target for BAP1-deficient malignant mesothelioma. Cell Death Discov. *9*, 257. https://doi.org/10.1038/s41420-023-01552-5.
52. Takahashi, M., Ota, A., Karnan, S., Hossain, E., Konishi, Y., Damdindorj, L., Konishi, H., Yokochi, T., Nitta, M., and Hosokawa, Y. (2013). Arsenic trioxide prevents nitric oxide production in lipopolysaccharide -stimulated RAW 264.7 by inhibiting a TRIF-dependent pathway. Cancer Sci. *104*, 165–170. https://doi.org/10.1111/cas.12053.
53. Alberich-Jordà, M., Wouters, B., Balastik, M., Shapiro-Koss, C., Zhang, H., Di Ruscio, A., Radomska, H.S., Ebralidze, A.K., Amabile, G., Ye, M., et al. (2012). C/EBPγ deregulation results in differentiation arrest in acute myeloid leukemia. J. Clin. Invest. *122*, 4490–4504. https://doi.org/10.1172/JCI65102.
54. Long, D., Yang, B., Yang, M., Xiong, F., Zhu, X., Tan, Y., and Wu, H. (2023). Bach2 in CD4+ T cells from SLE patients modulates B-cell differentiation and IgG production. Eur. J. Immunol. *53*, e2250109. https://doi.org/10.1002/eji.202250109.
55. Zhang, B., Vogelzang, A., Miyajima, M., Sugiura, Y., Wu, Y., Chamoto, K., Nakano, R., Hatae, R., Menzies, R.J., Sonomura, K., et al. (2021). B cell-derived GABA elicits IL-10. Nature *599*, 471–476. https://doi.org/10.1038/s41586-021-04082-1.

STAR★METHODS

KEY RESOURCES TABLE

REAGENT or RESOURCE	SOURCE	IDENTIFIER
Antibodies		
anti-human RP105	This paper	kindly provided by Dr. Kensuke Miyake, the University of Tokyo
anti-human CD3-APC/Cy7	Biolegend	Biolegend, Cat#344818
anti-human CD14-PE	Biolegend	Biolegend, Cat#301806
anti-human CD19-APC	Biolegend	Biolegend, Cat#392504
anti-human CD19-PE	Biolegend	Biolegend, Cat#302208
anti-human CD20-APC	Biolegend	Biolegend, Cat#302310
anti-human CD27-APC	Biolegend	Biolegend, Cat#302810
anti-human CD38-PE/Cy7	Biolegend	Biolegend, Cat#303516
anti-human CD80-APC	Biolegend	Biolegend, Cat#375404
anti-human IgD-FITC	Biolegend	Biolegend, Cat#348206
anti-human RP105-PE/Cy7	Biolegend	Biolegend, Cat#312910
anti-human IL-6R antibody	Absolute Biotech Company	Absolute Biotech Company, Cat#Ab00737–10.0
Hashtag oligo, TotalSeq-C0251	Biolegend	Biolegend, Cat#394661
Hashtag oligo, TotalSeq-C0252	Biolegend	Biolegend, Cat#394663
Hashtag oligo, TotalSeq-C0253	Biolegend	Biolegend, Cat#394665
Hashtag oligo, TotalSeq-C0254	Biolegend	Biolegend, Cat#394667
Hashtag oligo, TotalSeq-C0255	Biolegend	Biolegend, Cat#394669
Hashtag oligo, TotalSeq-C0256	Biolegend	Biolegend, Cat#394671
biotin-conjugated anti-human IgG	Jackson ImmunoResearch	Jackson ImmunoResearch, Cat#109-066-003
biotin-conjugated anti-human IgM	Jackson ImmunoResearch	Jackson ImmunoResearch, Cat#109-065-043
Goat Anti-Human IgG-HRP	Southern Biotechnology	Southern Biotechnology, Cat#2040-05
Goat Anti-Human IgA-HRP	Invitrogen,	Invitrogen, Cat#627420
Chemicals, peptides, and recombinant proteins		
Histopaque®-1077	Sigma-Aldrich	Sigma-Aldrich, Cat#10771-500ML
5-(and-6)-carboxyfluorescein diacetate, succinimidyl ester	Invitrogen	Invitrogen, Cat#C1157
RPMI1640	Sigma-Aldrich	Sigma-Aldrich, Cat#ML8758-500R
AIM-V medium	Gibco	Gibco, Cat#12055-091
CpGDNA	Miltenyi Biotec	Miltenyi Biotec, Cat#130-100-105
Transthyretin	MyBioSource	MyBioSource, Cat#MBS173179
Haptoglobin	MyBioSource	MyBioSource, Cat#MBS844021
Hemopexin	MyBioSource	MyBioSource, Cat#MBS170373
chloroform	FUJIFILM Wako Pure Chemical Corporation	FUJIFILM Wako, Cat#033-08631
methanol	FUJIFILM Wako Pure Chemical Corporation	FUJIFILM Wako, Cat#138-18541
acetonitrile	FUJIFILM Wako Pure Chemical Corporation	FUJIFILM Wako, Cat#016-26221
formic acid	FUJIFILM Wako Pure Chemical Corporation	FUJIFILM Wako, Cat#067-04531

(*Continued on next page*)

Continued

REAGENT or RESOURCE	SOURCE	IDENTIFIER
Trypsin/Lys-C Mix, Mass Spec Grade	Promega	Promega, Cat#V5071
acetic acid	FUJIFILM Wako Pure Chemical Corporation	FUJIFILM Wako, Cat#018-20061
Ultrapure Water	FUJIFILM Wako Pure Chemical Corporation	FUJIFILM Wako, Cat#212-01601
Iodoacetamide	FUJIFILM Wako Pure Chemical Corporation	FUJIFILM Wako, Cat#018-20061
Tris(2-carboxyethyl) phosphine	Sigma-Aldrich	Sigma-Aldrich, Cat#C4706
Blood Group A-BSA, 6-Atom Spacer	Dextra Laboratories, Ltd	Dextra, Cat#NGP6305
Blood Group B-BSA, 6-Atom Spacer	Dextra Laboratories, Ltd	Dextra, Cat#NGP6323
Galα1-3Galβ1-4GlcNAc-BSA, 3 atom spacer	Dextra Laboratories, Ltd	Dextra, Cat#NGP0334
SARS CoV-2 Wuhan-Hu-1 S1 protein with His tag	Acro Biosystems	Acro Biosystems, Cat#S1N-C52H3
Streptavidin-Horseradish Peroxidase (HRP) Conjugate	Invitrogen	Invitrogen, Cat#SA10001
KOD FX *Neo* polymerase	Toyobo	Toyobo, Cat#KFX-201
Critical commercial assays		
CD19 MicroBeads, human	Miltenyi Biotec	Miltenyi Biotec, Cat#130-050-301
Naive B Cell Isolation Kit II, human	Miltenyi Biotec	Miltenyi Biotec, Cat#130-091-150
Memory B Cell Isolation Kit, human	Miltenyi Biotec	Miltenyi Biotec, Cat#130-093-546
iST kit	PreOmics	PreOmics, Cat#P.O.00173
C18W-3 trap column (0.5 × 1 mm)	KYA	KYA, Cat#A03-05-001
C18HS-3 (0.1 × 100 mm)	KYA	KYA, Cat#E03-100-100
Pierce C18 Spin Tips	Thermo Scientific	Thermo Scientific, Cat#84850
nanoEase™ M/Z Peptide CSH C18 column	Waters	Waters, Cat#186008810
Chromium Next GEM Single Cell 5′ Kit v2	10x Genomics	10x Genomics, Cat#PN-1000263
Chromium Next GEM Chip K Single Cell Kit	10x Genomics	10x Genomics, Cat#PN-1000287
Dual Index Kit TT Set A	10x Genomics	10x Genomics, Cat#PN-1000215
5′ Feature Barcode Kit	10x Genomics	10x Genomics, Cat#PN-1000256
Dual Index Kit TN Set A	10x Genomics	10x Genomics, Cat#PN-1000250
High-Sensitivity DNA Kit	Agilent	Agilent, Cat# 5067-4626
SPRIselect magnetic beads	Beckman-Coulter	Beckman-Coulter, SPRIselect, Cat# B23317
1-Step Ultra TMB-ELISA	Thermo Fisher Scientific	Thermo Fisher Scientific, Cat#34028
CellTiter 96® AQueous One Solution Cell Proliferation Assay	Promega	Promega, Cat#G3582
RNeasy micro Kit	Qiagen	Qiagen, Cat#74004
TaqMan™ Gene Expression Assay	Toyobo	Toyobo, Cat#FSQ-201
Thunderbird probe qPCR mix	Toyobo	Toyobo, Cat#QPS-101
Deposited data		
human UniProt database	This paper	UP000005640: https://www.uniprot.org/proteomes/UP000005640
Proteome Xchange Consortium via jPOSTrepo	This paper	JPST002072: https://repository.jpostdb.org/
NCBI Gene Expression Omnibus (GEO)	This paper	GSE241135
Software and algorithms		
FlowJov10.7.2	FlowJo LLC	https://www.flowjo.com/
IncuCyte S3 software	Sartorius	https://www.sartorius.com/en
ProteinPilot software v5.02	Sciex	https://sciex.jp/
MarkerView Software	Sciex	https://sciex.jp/

(*Continued on next page*)

Continued

REAGENT or RESOURCE	SOURCE	IDENTIFIER
DIA-NN44 25, 1.8.1	DIA-NN github repository	https://github.com/vdemichev/DiaNN
cellranger 6.0.0	10x Genomics	https://www.10xgenomics.com/jp
Seurat 4.0.6	R	https://satijalab.org/seurat/
GraphPad Prism 5	GraphPad Software Inc.	https://www.graphpad.com/
Equipment		
IncuCyte ZOOM™	Sartorius	https://www.sartorius.com/en
nanoLC systems DiNA W, DiNA ASM	Techno Alpha Co.,	https://www.technoalpha.co.jp/
Sciex Triple TOF 5600	Sciex	https://sciex.jp/
nanoLC systems ACQUITY UPLC M-Class	Waters	https://www.waters.com/nextgen/jp/ja.html
Sciex ZenoTOF7600	Sciex	https://sciex.jp/
FACS Aria III	BD Biosciences	https://www.bdbiosciences.com/ja-jp
Veriti Thermal Cycler	Thermo Fisher Scientific	https://www.thermofisher.com/jp/ja/home.html
Agilent Bioanalyzer	Agilent	https://www.chem-agilent.com/index.php
MGI DNBSEQ-G400	MGI Tech Japan	https://jp.mgi-tech.com/
Novocyte	Agilent	https://www.chem-agilent.com/index.php
SpectraMax M5	Molecular Devices	https://www.moleculardevices.co.jp/
QuantStudio™ 3 Real-time PCR system	Thermo Fisher Scientific	https://www.thermofisher.com/jp/ja/home.htm

RESOURCE AVAILABILITY

Lead contact

Further information and requests for resources and reagents should be directed to and will be fulfilled by the lead contact, Kenta Iwasaki (kentaiwasaki@aichi-med-u.ac.jp).

Materials availability

Materials are available via contact with the corresponding author/lead contact.

Data and code availability

- The mass spectrometry proteomics data have been deposited to the human UniProt database and Proteome Xchange Consortium via jPOSTrepo with the dataset identifiers UP000005640: https://www.uniprot.org/proteomes/UP000005640 and JPST002072: https://repository.jpostdb.org/.
- Additional information needed to analyze the data reported in this paper is available upon request from the lead contact.
- Raw single cell RNA sequencing reads were deposited in the NCBI Gene Expression Omnibus (GEO) database under the accession number GSE241135.

EXPERIMENTAL MODEL AND STUDY PARTICIPANT DETAILS

Human subjects

Fresh peripheral blood mononuclear cells (PBMCs) were obtained from healthy volunteers who had previously received the two or three-dose regimen of either the Moderna (mRNA-1273) or Pfizer-BioNTech (BNT162b2) mRNA vaccine against the WT (Wuhan-Hu-1) strain of SARS-CoV-2, and kidney transplant recipients. Also, written informed consent was obtained from healthy volunteers and kidney transplant recipients. The Institutional Ethics Committees of Aichi Medical University School of Medicine approved this study (15–092, 15-H072, 16-M004). The research was performed by all relevant guidelines and regulations. Blood samples were subjected to FCM analysis. PBMCs were obtained from whole blood through density gradient centrifugation using Ficoll-Paque (Sigma-Aldrich, St. Louis, MO). PBMCs were stored in nitrogen tanks until used in experiments.

METHOD DETAILS

In vitro B-cell proliferation assay (carboxyfluorescein diacetate, succinimidyl ester (CFSE)-based cell proliferation assay)

Cryopreserved PBMCs were stained with carboxyfluorescein diacetate, succinimidyl ester (CFSE). $CD19^+$ B-cells were isolated using MACS LS Columns for $CD19^+$ B-cells magnetic cell negative isolation kits (Miltenyi Biotec, Bergisch Gladbach, Germany). A total of 1×10^5 cells (either

PBMCs or purified B-cells)/100 μL/well was cultured in RPMI1640 (Sigma-Aldrich) supplemented with 10% fetal bovine serum (FBS) or AIM-V medium (Thermo Fisher Scientific, Waltham, MA) supplemented with 10% FBS and HEPES (Dojindo, Kumamoto Japan). First, the culture medium was reviewed based on previous reports[30]: two culture mediums (RPMI1640 containing 10% FBS and AIM-V medium containing 10% FBS and HEPES) were prepared and each was evaluated for $CD19^+$ B-cell proliferative potential upon stimulation with αhRP105. PBMCs were stained with CFSE and cultured for 3days after αhRP105 stimulation. Gating strategy and $CD19^+$ B-cells proliferation were assessed using FCM (Figure 1A). Figure 1B showed representative CFSE discrete peaks which represented successive generations of live cells. Cells were stimulated with αhRP105 (kindly provided by Dr. Kensuke Miyake, the University of Tokyo), CpGDNA (Miltenyi Biotech, Invivogen), Transthyretin (MyBioSource, Vancouver, Canada), Haptoglobin (MyBioSource), and/or Hemopexin (MyBioSource), followed by staining with anti-human CD19-PE, CD80-APC, and CD38-PE/Cy7 antibodies (all from Biolegend, San Diego, CA). Cell proliferation was analyzed after 3days of incubation using FlowJo software (FlowJo LLC, Ashland, OR). The mitotic index and stimulation index were calculated as previously reported.[47]

In vitro naive (IgD^+CD27^-) and memory ($CD27^+$) B-cells proliferation assay (MTS-based cell viability assay)

$CD19^+$ naive (IgD^+CD27^-) and memory ($CD27^+$) B-cells were isolated using MACS LS Columns for magnetic cell negative or positive isolation kits respectively (Miltenyi Biotec). A total of 2×10^4 cells/100 μL/well was cultured in AIM-V medium (Thermo Fisher Scientific) supplemented with 10% FBS and HEPES. Cells were stimulated with αhRP105 and/or CpGDNA. Cell proliferation was analyzed after 3days of incubation using CellTiter 96 AQueous One Solution Cell Proliferation Assay (Promega, Madison, WI) according to the manufacturer's instructions with minor modifications. Briefly, 75 μL of the supernatant was discarded and 5 μL of MTS reagent was added, followed by incubation for 5h. The absorbance at 490–630 nm wavelength using a 96-well plate reader were recorded.

In vitro cluster formation of B-cells

CFSE-stained purified $CD19^+$ B-cells in AIM-V containing 10% FBS and HEPES were seeded onto 96-well cell culture plates and incubated with αhRP105 for several days in the IncuCyte ZOOM live cell imaging system (Essen BioScience, Tokyo, Japan) to measure cell cluster formation (Objectives: 4×, Image resolution: 3.05 μm/pixel, Fluorescence excitation/emission: Green 440–480 nm). The system automatically captures the images within the initially vacant area at 5 min intervals over 3days. Changes over time to the formation of cell clusters are shown in the supplemental information as a movie. Cell clusters were defined as those with 20 μm or more and their numbers were counted. Data were exported and analyzed by IncuCyte S3 software (Essen Bioscience).

LC/ESI-MS/MS and DDA-MS data analysis

AIM-V media (200 μL) were mixed with 400 μL of a chloroform/methanol (2:1, v/v) solution; the resulting mixture was vigorously agitated for 1 min then centrifuged at 20,000 × g for 10 min and the aqueous phase was removed. The remaining precipitate and organic phases were then mixed with 200 μL of chloroform, and the resulting mixture was centrifuged at 20,000 × g for 10 min to obtain the proteins. Proteins (10 μg) were digested using the iST kit (PreOmics, Germany). The digested samples were then evaporated to dryness *in a vacuo* to give the residues. These residues were dissolved in 10 μL of 2% acetonitrile, 5% formic acid in water, and 1 μL of injected onto nanoLC/ESLI-MS/MS systems [nanoLC: DiNa-ASM and DiNa-W (Techno Alpha Co., Ltd., Tokyo, Japan), MS: Sciex TripleTOF 5600 (Sciex, MA, USA)]. The peptide samples were separated using a C18W-3 trap column (0.5 × 1 mm) and C18HS-3 (0.1 × 100 mm) (Techno Alpha) at a flow rate of 300 nL/min with the following gradient: 0–2 min: 0–5% solvent B (0.1% formic acid in acetonitrile), 2–90 min: 45% B, 90–105 min: 100% B, 105–130 min: 100% buffer A (2% ACN, 0.1% FA). The mass spectrometer was operated in data-dependent analysis (DDA) top 20 positive ion mode, with 250 and 100 ms acquisition time for the MS1 (*m/z* 400–1500) and MS2 (*m/z* 230–1800) scans respectively. The raw MS data were processed with ProteinPilot software v5.02 (Sciex). The Scaffold DDA search parameter as follows: human spectral library, human UniProt database (id UP000005640, reviewed, canonical) experimental data search enzyme, trypsin; static modification, carbamidomethylation of cysteine residues; dynamic modification, oxidation of methionine. The protein identification threshold was set at <1% for both peptide and protein False Discovery Rate (FDR).

Zeno SWATH-MS data acquisition

Human B-cell protein samples (10 μg) were dissolved in 8 M urea in 50 mM Tris-HCl, pH 8. Protein samples were reduced with 2 mM Tris(2-carboxyethyl) phosphine for 60 min at 37°C and carbamidomethylated with 5 mM iodoacetamide for 60 min in the dark at room temperature before diluting the sample with 50 mM Tris-HCl, pH 8 to a final urea concentration below 0.8 M. Proteins were digested with trypsin/Lys-C (1/25, enzyme/protein) overnight at 37°C. Trypsin/Lys-C was inactivated by lowering pH 2–3 with formic acid. The digested samples were cleaned up using Pierce C18 Spin Tips (Pierce). and evaporated to dryness *in a vacuo* to give the residues. These residues were dissolved in 10 μL of 2% acetonitrile, 5% acetic acid in water, and 1 μL of injected into nanoLC/ESLI-MS/MS systems [LC: ACQUITY UPLC M-Class system (Waters, MA, USA), MS: ZenoTOF7600 (Sciex)]. The peptide samples were separated using nanoEase M/Z Peptide CSH C18 column (1.7 μm, 0.075 × 150 mm) (Waters) at a flow rate of 300 nL/min. Mobile phase A consisted of a 0.1% (v/v) solution of formic acid in water, and mobile phase B consisted of a 0.1% (v/v) solution of formic acid in acetonitrile. The linear gradient conditions were as follows: 0–17 min: 2% solvent B, 17–125 min: 30% B, 126–127 min: 40% B, 127–132 min: 80% B, 132–133 min: 90% B, 133–153 min: 90% B, 153–154 min: 2% B, 154–180 min: 2% B. The mass spectrometer was operated in a Zeno SWATH acquisition scheme with 100 variable-size windows and 25 ms accumulation time was

used. The Zeno SWATH raw MS data were processed using DIA-NN 1.8.1,[48] available on github (DIA-NN github repository). The human spectral libraries were generated from the human spectral library, human UniProt database (id UP000005640, reviewed, canonical). The DIA-NN search parameters were as follows: experimental data search enzyme, trypsin; missed cleavage sites, 1; peptide length range, 7–30; precursor mass charge range, 1–4; precursor *m/z* range, 300–1800; fragment ion *m/z* range, 200–1800; and static modification, cysteine carbamidomethylation. The protein identification threshold was set at <1% for both peptide and protein FDR. The protein expression trends were analyzed using principal component analysis-discriminant analysis (PCA-DA) in MarkerView Software (Sciex). The newly acquired mass spectrometry proteomics data have been deposited to the Proteome Xchange Consortium via jPOSTrepo with the dataset identifier JPST002072.

Single-cell RNA library construction and sequencing

For scRNA-seq analysis, PBMCs were stimulated with αhRP105 for 36h in AIM-V containing 10% FBS and HEPES, then were stained with cell hashtag oligos (HTOs) antibody, TotalSeq-C0251 to -C0256 together with antni-CD19-PE and anti-CD20-APC (all from Biolegend). $CD19^+CD20^+$-gated population as B-ells were sorted by FACS Aria III (BD Biosciences, Franklin Lakes, NJ) and used for scRNA-seq analyses. Single-cell suspensions were processed through the 10x Genomics Chromium Controller following the protocol outlined in the Chromium Single Cell 5′ Reagent Kits v2 User Guide. Chromium Next GEM Single Cell 5′ Kit v2 (Cat#PN-1000263), Chromium Next GEM Chip K Single Cell Kit (Cat#PN-1000287), Dual Index Kit TT Set A (Cat#PN-1000215), 5′ Feature Barcode Kit (Cat# PN-1000256) and Dual Index Kit TN Set A (Cat#PN-1000250) were applied during the process. Approximately 16,500 live cells per sample, according to the manufacturer's recommendations, were loaded onto the Chromium controller to generate 10,000 single-cell gel-bead emulsions for library preparation and sequencing. Oil droplets of encapsulated single cells and barcoded beads were subsequently reverse-transcribed in a Veriti Thermal Cycler (Thermo Fisher Scientific), resulting in mRNA-derived cDNA and HTO-derived cDNA tagged with a cell barcode and unique molecular index. Next, cDNA was then amplified to generate single-cell libraries according to the manufacturer's protocol. Quantification was made with an Agilent Bioanalyzer High Sensitivity DNA assay (Agilent, High-Sensitivity DNA Kit, Cat#5067-4626). Subsequently amplified cDNA was enzymatically fragmented, end-repaired, and polyA tagged. Cleanup/size selection was performed on amplified cDNA using SPRIselect magnetic beads (Beckman-Coulter, SPRIselect, Cat#B23317). Next, Illumina sequencing adapters were ligated to the size-selected fragments and cleaned up using SPRIselect magnetic beads. Finally, sample indices were selected and amplified, followed by a double-sided size selection using SPRIselect magnetic beads. For cell hashing feature barcode libraries were constructed with HTO-derived cDNA. Final library quality was assessed using an Agilent Bioanalyzer High Sensitivity DNA assay. Samples were then sequenced on MGI DNBSEQ-G400 as paired-end mode (2 × 100 nt). The resulting raw reads were processed by cellranger 6.0.0 (10x Genomics). Raw sequencing reads were deposited in the NCBI Gene Expression Omnibus (GEO) database under the accession number GSE241135. Normalization and downstream analysis of the scRNA-seq data were analyzed using the Seurat 4.0.6 workflow for demultiplexing with HTO.[49,50] Briefly, after classifying each cell as positive or negative for each HTO, cells that were positive for more than one HTOs were annotated as doublets and removed. Only cells assigned a single hashtag were kept for the following analyses. B cell activation markers (CD27, CD38, CD80, CD86, and CD40), TLR family members (TLR1, TLR2, TLR3, TLR4, TLR5, TLR6, TLR7, TLR8, TLR9, TLR10, LY86 (RP105), and LY96), IL-6 related genes (IL6R and IL6ST (encoding gp130)), cell cycle genes (OCND1, OCND2, CDK1, CDK2, CDK3, CDK4, PCNA, CDKN1A, CDKN2A, CDKN1B, SMAD3, and FOXO1), NF-κB family members (IKBKG, CHUK, IKBKB, NFKB1A, NFKB1, NFKB2, RELA, and RELB), memory B-cell-related genes (BACH2, PRDM1, IL9R, BCL6, SDC1, CD138, CR2, TNFRSF13C, and TNFRSF13B), and C/EBPγ were analyzed.

Measurement of hRP105 expression on human B-cells

Cryopreserved PBMCs from healthy volunteers and transplant recipients were stained with anti-CD3-APC/Cy7, anti-CD14-PE, anti-CD19-APC or PE, anti-IgD-FITC, anti-CD27-APC, and anti-RP105-PE/Cy7 (all from Biolegend), and were subject to Novocyte (Agilent, Santa Clara, CA). Each molecule's expression was analyzed using FlowJo software.

Quantitative real-time PCR (qRT-PCR)

Total RNA was extracted from cells using RNeasy micro Kit (Qiagen, Hilden, Germany) and was reverse-transcribed using ReverTra Ace (Toyobo, Tokyo, Japan) according to the manufacturer's instructions. The gene expression level of PRDM1 was determined using TaqMan Gene Expression Assay (Hs00153357_ml, Thermo Fisher Scientific) and Thunderbird probe qPCR mix (Toyobo) reagents and normalized to the level of β-actin (Hs01060665_g1). The level of GAPDH and CEBPG was also determined using SYBR Green I (TaKaRa, Tokyo, Japan) and KOD FX *Neo* polymerase (Toyobo) reagents and normalized to that of 18S rRNA as previous described.[51,52] The primer sequences were indicated as follows; CEBPG F: 5′-GGCTAGAGGAGCAGGTACAT-3′, R: 5′- GCCTGGGTATGGATAACACTA-3′,[53] GAPDH F: 5′-GGAGCGAGATCCCTCCAAAAT-3′, R: 5′-GGCTGTTGTCATACTTCTCATGG-3′,[54] 18S rRNA F: 5′-GGCCCTGTAATTGGAATGAGTC-3′, R: 5′-CCAAGATCCAACTACGAGCTT-3′.[55] All quantitative analysis was performed using the QuantStudio 3 Real-time PCR system. All data analyses were performed using Design & Analysis software version 2.8.

In vitro antibody production from $CD19^+$ B-cells stimulated with αhRP105 and CpGDNA

$CD19^+$ B-cells were negatively isolated using MACS LS Columns for magnetic cell isolation with MicroBeads (Miltenyi Biotec). Naive (IgD^{+-} $CD27^-$) and memory human B-cells ($CD27^+$) were separated by FACS Aria III using CD27 and IgD as markers. A total of 1×10^5 cells/100 μL/well in in AIM-V containing 10% FBS and HEPES medium were activated with αhRP105 and CpGDNA. After incubation for 2days or 10days in

5% CO_2 at 37°C, the supernatant of cultured cells was subjected to Enzyme-linked immunosorbent assay (ELISA) to detect total IgG (IgG1, IgG2, IgG3, and IgG4), total IgM, total IgA, anti-ABO blood type antibody, anti-αGal antibody, anti-SARS-CoV-2 S1 antibody. Anti-IL-6R antibody (rabbit IgG recombinant mAb, clone rhPM-1, Absolute Biotech Company, Wilton, UK) was used for the inhibition assay.

Enzyme-linked immunosorbent assay (ELISA)

Dilute unlabeled capture antibody (anti-IgG, anti-IgM, anti-IgA, anti-blood A, anti-blood B, anti-αGal, anti-IL-6 and anti-human IgG for sandwich ELISA; Biolegend, Bethyl Laboratories) and recombinant SARS CoV-2 Wuhan-Hu-1 S1 protein with His tag (Acro Biosystems, Tokyo, Japan) to a final concentration of 2.5 μg/mL in PBS or carbonate-bicarbonate buffer was transferred into each well of ELISA plate (IWAKI, Shizuoka, Japan), and was incubated at 4°C overnight. The plate was incubated with Tris-buffered saline containing bovine casein (Merck Millipore, Darmstadt, Germany) for blocking for 1h. The plate was then incubated with serially diluted supernatants or serum. After additional 3 times washing with PBS-T (PBS+0.05% Tween 20), dilute standards and samples to desired concentrations were added to the plate, followed by incubation at room temperature for 1-4h or at 4°C overnight. After 3 times washing with PBS-T, biotin-conjugated antibody (anti-human IgG, IgG1, IgG2, IgG3, and IgG4 (Jackson ImmunoResearch, West Grove, PA) anti-human IgM (Jackson ImmunoResearch), anti-blood A, anti-blood B, anti-αGal, anti-IL-6), HRP-conjugated anti-human IgG (Southern Biotechnology), or anti-human IgA (Invitrogen), was added, then the plated was incubated at room temperature for 1h. After 3 times washing with PBS-T, avidin-Horseradish Peroxidase was added, followed by incubation at room temperature for 30 min. After 3 times washing with PBS-T, 1-Step Ultra TMB-ELISA (Thermo Fisher Scientific) was added for color development. To stop the color reaction, add 50 μL of water Stop Solution. Read the optical density (OD) for each well with SpectraMax M5 (Molecular Devices, CA, USA) or SpectraMax ABS Plus to 405 nm or 450 nm.

Statistical analysis

The results are presented as mean ± standard error of the mean. Analyses were performed using GraphPad Prism 5 (GraphPad Software, Inc. La Jolla, CA). Furthermore, statistical analyses were performed using Student *t*, Steel–Dwass, Mann–Whitney, one-way ANOVA, or Kruskal–Wallis tests. A *p*-value of <0.05 was considered statistically significant.